Reconfigurable antennas and radio wave propagation at millimeter-wave frequencies

Vasilii Semkin

A? Aalto University

Reconfigurable antennas and radio wave propagation at millimeter-wave frequencies

Vasilii Semkin

A doctoral dissertation completed for the degree of Doctor of Science (Technology) to be defended, with the permission of the Aalto University School of Electrical Engineering, at a public examination held at the lecture hall S4 of the school on 2 September 2016 at 12.

Aalto University
School of Electrical Engineering
Department of Radio Science and Engineering

Supervising professor
Prof. Antti V. Räisänen, Aalto University, Finland

Thesis advisors
Prof. Dr.-Ing. Thomas Kürner, Technische Universität Braunschweig, Germany
Dr. Juha Ala-Laurinaho, Aalto University, Finland

Preliminary examiners
Prof. Dr.-Ing. Thomas Zwick, Karlsruher Institut für Technologie, Germany
Prof. Özlem Aydin Civi, Middle East Technical University, Turkey

Opponent
Prof. Lluís Jofre, Universitat Politècnica de Catalunya, Spain

441   697
Printed matter

Abstract

For the last decades we have been witnessing the evolution of wireless radio networks. Since new devices appear and the mobile traffic, as well as the number of users, grows rapidly, there is a great demand in high capacity communications with better coverage, high transmission quality, and more efficient use of the radio spectrum. In this thesis, reconfigurable antennas at micro- and millimeter-wave frequencies and peculiar properties of radio wave propagation at mm-wave frequencies are studied.

Reconfigurable antennas can improve radio link performance. Recently, many different concepts have been developed in the reconfigurable antenna design to control the antenna bandwidth, resonant frequency, polarization, and radiation properties. In the first part of the thesis, we investigate mechanically tunable antennas operating at microwave frequencies with the ability to change the shape of the conductor element and, consequently, to control the radiation properties of the antenna. Also in the first part, we study conformal antenna arrays for 60 GHz applications based on cylindrical structures. Beam switching technology is implemented by realizing several antenna arrays around the cylinder with a switching network. Scanning angles of +34˚/-32˚ are achieved.

Moreover, it is vital to study radio wave propagation peculiarities at mm-wave frequencies in indoor and outdoor environments to be able to deploy wireless networks effectively. The propagation part of the thesis focuses on several aspects. First, we investigate how the estimation of optimum antenna configurations in indoor environment can be done using realistic propagation models at 60 GHz. Ray tracing simulations are performed and realistic human blockage models are considered. Second, we present the results from a measurement campaign where reflection and scattering properties of two different built surfaces are studied in the millimeter-wave E-band (71-76 and 81-86 GHz). Next, we present a geometry based channel model for a street canyon scenario, using angular-domain measurement results to calculate realistic power angular spectra in the azimuth and elevation planes. Then, we evaluate propagation effects on the radio channel on the rooftop of the buildings by measurements and simulations. We have used unmanned aerial vehicles and photogrammetry technique to create a highly accurate 3D model of the environment. Based on a comparison of the measured and simulated power delay profiles, we show that the highly accurate 3D models are beneficial in radio wave propagation planning at mm-wave frequencies instead of using simple geometrical models.

Preface

The doctoral thesis has been carried out in the Department of Radio Science and Engineering at Aalto University, School of Electrical Engineering. I am very grateful to my first supervisor, late Prof. Pertti Vainikainen, who gave me an opportunity to become a PhD student in his group, for his invaluable support and guidance in my doctoral studies and fruitful discussions during which I have learnt a lot about radio communications. I am very thankful to Prof. Antti Räisänen who became my supervisor in August 2012 for his great help and support during my doctoral studies.

I want to thank my former instructors Dr. Veli-Matti Kolmonen and Dr. Mikko Kyrö for their priceless advices, ideas for the research work and help during my studies. I would like to thank my instructors Prof. Thomas Kürner and Dr. Juha Ala-Laurinaho for their useful advices and discussions. I would also like to thank Prof. Sergei Tretyakov for sharing his ideas and experience, which helped to improve the results of this work.

I express my gratitude to Prof. Cyril Luxey, Associate Prof. Fabien Ferrero and Dr. Aimeric Bisognin, for their instructions during my research visits to Nice in 2012 and 2014 and also for their cooperation during my doctoral research. Furthermore, my thanks go to Prof. Thomas Kürner and Dr. Martin Jacob for hosting and instructing me during my research visit to Braunschweig in 2013. I would like to thank my former colleague Oleg Platonov for numerous interesting discussions and our collaboration. Also my current and former colleagues at the Department of Radio Science and Engineering deserve warm thanks for their support and informal discussions. Thanks to Dr. Risto Valkonen, Dr. Dmitry Morits, Dr. Andrey Generalov, Lic. Sc. Irina Nefedova, Dr. Igor Nefedov, Dr. Ilya Anoshkin, Prof. Katsuyuki Haneda, Dr. Aki Karttunen, Mr. Reza Naderpour, Mr. Usman Virk, Mr. Jan Järveläinen, Dr. Joni Vehmas, Mr. Kimmo Rasilainen, and many others. I would also like to thank my co-author Mr. Dmitrii Solomitckii from Tampere University of Technology.

I would like to thank the pre-examiners, Prof. Thomas Zwick and Prof. Özlem Aydin Civi, for their valuable comments and suggestions for improving this thesis.

Thanks to my parents Marina and Viktor, and my grandparents Vladimir and Rimma for the support and encouragement.

Finally, I send my warmest thanks to my wife Karina for your love, patience and support during last years of my studies.

Espoo, July 26, 2016,

Vasilii Semkin

Contents

List of Publications

This thesis consists of an overview of the following publications which are referred to in the text by their Roman numerals.

I   V. Semkin, O. Platonov, M. Kyrö, and A. V. Räisänen, "Liquid metal patch antenna and antenna array for WLAN applications," *Microwave and Optical Technology Letters*, vol. 56, no. 10, pp. 2462-2464, Oct. 2014.

II   V. Semkin, A. Bisognin, M. Kyrö, V.-M. Kolmonen, C. Luxey, F. Ferrero, F. Devillers, and A. V. Räisänen, "Conformal antenna array for millimeter-wave communications: performance evaluation," *International Journal of Wireless and Microwave Technologies*, 2015, available online, doi:10.1017/S1759078715001282.

III V. Semkin, F. Ferrero, A. Bisognin, J. Ala-Laurinaho, C. Luxey, F. Devillers, and A. V. Räisänen, "Beam switching conformal antenna array for mm-wave communications," *IEEE Antennas and Wireless Propagation Letters*, vol. 15, pp. 28-31, 2016.

IV   V. Semkin, M. Jacob, T. Kürner, A. Bisognin, F. Ferrero, C. Luxey, and A. V. Räisänen, "Estimation of optimum antenna configurations supported by realistic propagation models at 60 GHz," *European Conference on Antennas and Propag. (EuCAP2014),* The Hague, The Netherlands, Apr. 2014, pp. 3434-3438.

V   M. Kyrö, V. Semkin, and V.-M. Kolmonen, "Empirical characterization of scattering pattern of built surfaces at mm-wave frequencies," *European Conference on Antennas and Propag. (EuCAP2013),* Gothenburg, Sweden, Apr. 2013, pp. 112-115.

VI   V. Semkin, U. Virk, A. Karttunen, K. Haneda, and A. V. Räisänen, "E-band propagation channel measurements in an urban street canyon," *The 9th European Conference on Antennas and Propagation (EuCAP 2015)*, Lisbon, Portugal, Apr. 2015.

VII V. Semkin, D. Solomitckii, R. Naderpour, S. Andreev, Y. Koucheryavy, and A.V. Räisänen, "Characterization of radio links at 60 GHz using simple geometrical and highly accurate 3D models," *submitted to IEEE Transactions on Vehicular Technology (original manuscript submitted 21.04.2016, under major revision at the time of printing the thesis)*, 2016.

Author's Contribution

I: "Liquid metal patch antenna and antenna array for WLAN applications"

The paper is based on the author's idea, and the author was responsible for manufacturing the antenna and for the content of the paper. Mr. Platonov assisted in the measurements. Dr. Kyrö and Prof. Räisänen supervised the work.

II: "Conformal antenna array for millimeter-wave communications: performance evaluation"

The author designed the antenna array and had the main responsibility for the manuscript. Dr. Kolmonen proposed the initial idea of the paper and supervised the work. Mr. Bisognin and Prof. Ferrero performed the measurements. Mr. Devillers manufactured the supporting structures for the antenna array. Prof. Luxey and Prof. Räisänen supervised the work.

III: "Beam switching conformal antenna array for mm-wave communications"

The main idea belongs to the author. The antenna array with the switch was designed by the author. The author was assisting in measurements, carried out by Prof. Ferrero and Dr. Bisognin. Mr. Devillers manufactured the supporting structures for the antenna array. Dr. Ala-Laurinaho, Prof. Luxey, and Prof. Räisänen supervised the work.

IV: "Estimation of optimum antenna configurations supported by realistic propagation models at 60 GHz"

The paper is based on the author's and Dr. Jacob's idea and the author was responsible for the ray tracing simulations and preparation of the manuscript. The author assisted Dr. Jacob in the development of a realistic propagation model. Prof. Kürner, Prof. Ferrero, Prof. Luxey, and Prof. Räisänen supervised the work.

V: "Empirical characterization of scattering pattern of built surfaces at mm-wave frequencies"

Dr. Kyrö had the main responsibility for developing the content of the paper. The author and Dr. Kyrö were the main responsible persons for carrying out the measurements. Dr. Kolmonen supervised the work.

VI: "E-band propagation channel measurements in an urban street canyon"

The author performed channel measurements with Mr. Virk and Dr. Karttunen. The author was responsible for preparation of the paper. The work was instructed by Prof. Haneda and Prof. Räisänen.

VII: "Characterization of radio links at 60 GHz using simple geometrical and highly accurate 3D models"

The author was responsible for developing the idea and content of the paper. The author, Mr. Solomotckii, and Mr. Naderpour prepared the manuscript. The measurements were performed by the author with the assistance of Mr. Naderpour. The highly accurate 3D model was created by the author. The author assisted Mr. Solomitckii in the shooting-and-bouncing ray simulations. Dr. Andreev, Prof. Koucheryavy, and Prof. Räisänen supervised the work.

List of abbreviations

2D	Two-dimensional
3D	Three-dimensional
APC	Antenna pattern comparison technique
AUT	Antenna under test
CPW	Coplanar waveguide
D/A control	Digital/analog control
DC	Direct current
FCC	United States Federal Communication Commissions
GO	Geometrical optics
GTD	Geometrical theory of diffraction
GSG	Ground-Signal-Ground
HD	High definition
HFSS	High frequency structure simulator
HPBW	Half power beam width
IC	Integrated circuit
IEEE	Institute of Electrical and Electronics Engineers
IM	Image method
LIDAR	Light Identification Detection And Ranging
LOS	Line-of-sight
MEMS	Microelectromechanical system
MKE	Multiple knife edge
mm-wave	Millimeter wave
PAS	Power angular spectrum
PCB	Printed circuit board

PDP	Power delay profile
PIN-diode	Diode with an undoped intrinsic semiconductor region between n- and p-type regions
PTFE	Polytetrafluoroethylene
RF	Radio frequency
RL	Ray launching
RT	Ray tracing
Rx	Receiver
SBR	Shooting-and-bouncing ray
SP3T	Single pole three throw (switch)
Tx	Transmitter
UAV	Unmanned aerial vehicle
UTD	Uniform theory of diffraction
VNA	Vector network analyzer
WLAN	Wireless local area network

List of symbols

c	Speed of light
dA, dA_o	Cross section areas
D_θ, D_φ	Directivity
$\boldsymbol{E}$	Electric field
f_r	Resonant frequency
G_{real}	Realized antenna gain
G_r	Receiving antenna gain
G_t	Transmitting antenna gain
h	Thickness of a substrate
$\boldsymbol{H}$	Magnetic field
L_{fs}	Free space loss
P_{rad}	Radiated power
P_r	Received power
P_t	Transmitted power
R	Distance between antennas
s	Distance between cross sections in an astigmatic tube of rays
$S_{11}, S_{12}, S_{21}, S_{22}$	Scattering parameters
U, U_o	Radiation power density
W	Patch width
α	Unideal factor in the scan loss
β	Propagation constant in free space
ε_r	Relative permittivity
$\varepsilon_{r\mathrm{eff}}$	Effective permittivity

η_0	Total antenna efficiency
θ	Spherical coordinate
θ_i	Angle of incidence
θ_r	Angle of reflection
θ_s	Scan angle
θ_t	Angle of transmission
λ	Wavelength
ρ	Curvature radius of the wave front
ρ_{rough}	Effective reflection coefficient
ρ_{smooth}	Reflection coefficient from a smooth surface
σ	Deviation of height distribution
φ	Spherical coordinate

1. Introduction

Since the first wireless systems appeared about 100 years ago, the data rates have dramatically increased. The rapid increase of mobile data transfer and appearance of new devices such as smartphones and tablets create increasing demands for the system designers. As the wireless access is nowadays considered as a reliable service, totally new usage scenarios have been invented at the same time as well. Many of these usage scenarios require responsive and reliable high-capacity communication systems. This goal is particularly challenging in densely populated areas, such as city centers. In these areas, the wireless systems have to be able to compensate for the increased interference levels and the core network has to be able to provide sufficient amount of throughput so that all customers can be served. It is difficult to achieve high data rates with the conventional radio systems because of limited bandwidth and limitations on the transmission power.

Wireless networks operating at millimeter-wave (mm-wave) frequencies are one of the promising solutions to support multi Gbit/s communications, thanks to the availability of a wide frequency spectrum. Moreover, due to the short wavelength, antennas operating at mm-wave frequencies can be integrated with the receivers and transmitters. The millimeter wave region corresponds to frequencies between 30 and 300 GHz with the wavelengths between 10 to 1 mm, respectively. In the wireless communications usually the term of mm-wave frequencies matches several bands of spectrum, such as 38, 60, 70-90, and 94 GHz. Also, the E-band (which consists of two frequency bands: 71-76 and 81-86 GHz) is already allocated for fixed point-to-point radio links [FCC2005, ETSI2006]. The main advantage of using such radio links is cost reduction comparing to the fiber optics systems. However, it is essential to know the peculiarities of mm-wave propagation since radio links can be affected by the propagation effects at these frequencies. At mm-wave frequencies the resonances of oxygen and water vapor molecules bring in additional losses and precipitation can cause high attenuation [FCC1997]. These effects mostly limit the use of certain mm-wave frequencies (especially around 60 GHz) to indoor scenarios. Compared with the lower frequency bands, millimeter wave radio signals can propagate only over shorter distances in the atmosphere. This is not a real drawback of such systems because they can provide high-speed communications for densely packed areas with more efficient spectrum utilization. One example of applications that require high data rate transmission in indoor environment is uncompressed high-quality video streaming. These communication systems are expected to provide more

than 1 Gbit/s data rate at distances up to 10 m. The 60 GHz frequency with a free-space wavelength of 5 mm makes the antenna structure physically compact. A bandwidth of 9 GHz available in the 60 GHz range makes co-channel interference less probable. High gain antenna arrays can be used to compensate for large free space losses. For indoor radio links human blockage can have a high impact on the radio channel [Singh2009, Jacob2011]. Smart antennas with high gain and beam steering capabilities can help to overcome the dynamic human blockage effects.

1.1. Objectives of this work

In a modern society a lot of digital content is being uploaded and downloaded from different digital services using wireless access. The increasing interest in high date rate communications brings new challenges for researchers. Reconfigurable antennas, with the ability to control their properties according to the changes in the environment, can help to improve the overall system performance and increase the system capacity. Furthermore, studies of radio wave propagation and channel modeling can help in careful planning and deployment of the wireless communication systems. In this thesis both of these relevant research topics are addressed.

The main objectives of this thesis are:

- To investigate the concept of reconfigurable microfluidic antennas for the usage in wireless local area networks.
- To develop a conformal antenna array operating at mm-wave frequencies, investigate its radiation performance and implement beam switching technology.
- To study the ray tracing method in order to envisage optimum antenna configurations for a specific environment based on the requirements for the communication system.
- To study radio wave propagation in the E-band in outdoor environments, including reflection and scattering properties of built surfaces and angular distribution of scatterers.
- To validate the applicability of highly accurate models of the environment for utilization in shooting-and-bouncing ray simulations.

1.2. Organization and contributions of the thesis

The structure of the thesis is illustrated in Figure 1.1. The figure presents the whole radio system, however, the thesis concentrates only on two topics: reconfigurable antennas for micro- and mm-wave communications (Chapter 2), and characterization of radio wave propagation at mm-wave frequencies (Chapter 3).
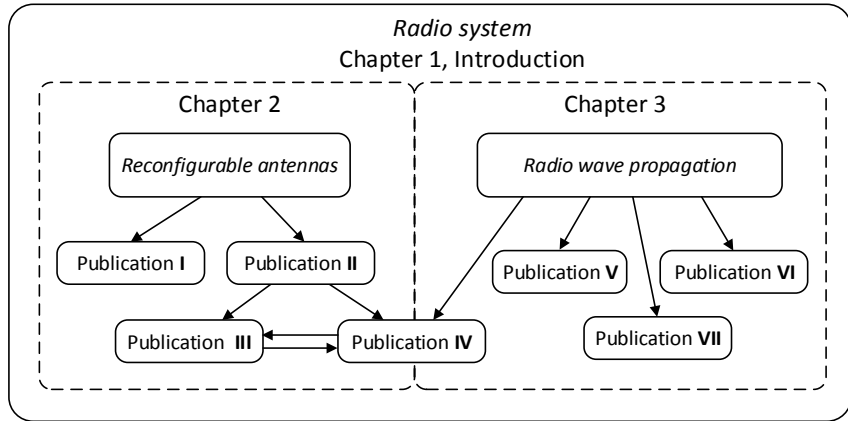
Figure 1.1. Illustration of the thesis content.

Chapter 2 of the thesis discusses different types of reconfigurable antennas. We investigate the applicability of various multi-element antenna configurations and manufacturing processes of these antennas for millimeter wave frequencies. A reconfigurable antenna is an antenna capable to modify dynamically its properties, e.g. the operational frequency or radiation pattern. Antennas with the ability to reconfigure their radiation patterns can be beneficial in high data rate wireless communication systems for frequency reuse and for mitigating interference. In the first part of Chapter 2, antenna structures operating at 5.8 GHz with the use of liquid metals such as gallium are investigated. Using the properties of liquid metals can help us to avoid the main disadvantages of mechanically-actuated reconfigurable antennas, for example, mechanical failures. Another advantage is that antenna arrays with liquid metal, forming the radiating part on a flexible substrate, can be deformable and mechanically tunable. Tunability and beam-steering capability can also be achieved by injecting liquid metal into appropriate channels in the antenna structure. Radiation properties of the antenna can be controlled and these antennas can dynamically adapt to the changes in the communication channel or in the system requirements.

Antenna operating at 5.8 GHz frequency can be used in wireless local area network (WLAN) applications to achieve higher data rate communications compared to the usual 2.4 GHz frequency band. The prototype of a microfluidic antenna was developed and measured in [**I**]. In the second part of Chapter 2, conformal antennas are investigated. Conformal antennas can have large impact on high data rate communications. One of the main advantages of using these antenna structures is that they replicate the form of an object on which they are placed. This can be a great benefit for mobile devices, which can have a curved shape, or in the flexible electronics. Conformal antennas can have high gain and quasi-omnidirectional radiation patterns for omnidirectional coverage, which is essential for mobile handheld or wearable devices. Beam steering or beam switching can be realized using such antenna structures. The performance of conformal antenna arrays for 60 GHz applications based on cylindrical structures were studied in paper [**II**].

Conformal antenna arrays with a beam switching network were developed and characterized; in [**III**].

Chapter 3 of the thesis deals with radio wave propagation modeling and channel measurements at mm-wave frequencies in outdoor and indoor environments. Publication [**IV**] relates to Chapter 2 and Chapter 3. Results obtained in [**IV**] indicate that preliminary information of optimum antenna configurations, in a conference room scenario, can be obtained by ray tracing simulations. Reconfigurable conformal antennas developed in [**II**] and described in the first part of the thesis are used in the ray tracing simulations. Moreover, it is shown that the first estimations of the optimum antenna parameters can be done approximating the antenna radiation patterns with Gaussian beam antenna patterns. Human blockage, which is one of the main attenuation factors at 60 GHz, is considered.

In order to deploy mobile networks effectively it is essential to know the characteristics of radio wave propagation in a certain environment. The information received from measurements can be used for implementing accurate channel models in realistic environments. Modeling radio wave propagation at millimeter-wave frequencies in urban environments requires knowledge of the reflection and scattering properties of built surfaces. The measured data has been used for characterization of such properties for brick and glass walls in [**V**].

E-band radio wave propagation in a street canyon scenario is characterized in [**VI**]. Based on the measurement results, an existing 2D channel model [Kyrö2012] is extended to a 3D model by using the angular distributions of scatterers. Realistic power angular spectra can be calculated using the presented channel model.

Finally, a measurement campaign has been carried out to evaluate propagation effects on a rooftop-to-rooftop radio channel. Two 3D models, obtained with different technologies, are presented: a simple geometrical model and a close-range photogrammetry model, which replicate the building geometry. The analysis is based on shooting-and-bouncing ray simulations and it aims at describing the feasibility of using highly accurate models of the environment in order to predict radio wave propagation effects at two different frequency bands [**VII**].

2. Reconfigurable antennas for smart radio systems

The 1st generation networks appeared in 1980's, they were analog and allowed only voice transmission. The first GSM network was launched in Finland by Radiolinja company in 1991. This digital cellular network of second generation (2G) allowed users to make calls and send text messages. Next, 2G system evolved into 2.5G and 2.75G with improvements in the data rates (56 kbit/s for 2.5G and 236 kbit/s for 2.75G, respectively) and services like Wireless Application Protocol (WAP), Multimedia messages (MMS) and Enhanced Data Rates for GSM Evolution (EDGE) technology were added [Lamba2012]. In 2002, 3G mobile networks based on Universal Mobile Telecommunication System (UMTS) technology appeared. This technology allows transmitting 14 Mbit/s of data. Later, 3G networks were developed to 3.5G and the data rates were increased up to 168 Mbit/s. LTE technology in the 4G mobile networks provides up to 337 Mbit/s of downlink speed. At the current time, 5G standard is being developed [Huawei2013, Bogale2016]. The primary goal is to support up to 1 Gbit/s for many users simultaneously. The main reasons for developing mobile networks are the increase in the data rates, appearances of new services and exponential growth of the number of connected devices. In Fig. 2.1 the forecast of the mobile traffic growth is presented [Cisco2016]. Mobile traffic data rates will exceed 30 Exabyte (1 Exabyte = 1 million of terabytes) per month by 2020. As can be seen, there is a great demand in high capacity communication systems which could support multi Gbit/s communications in the nearest future.
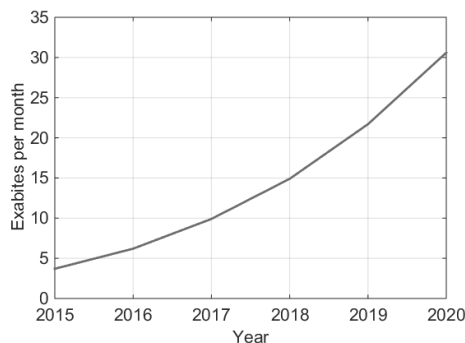

Figure 2.1. Mobile traffic forecast [Cisco2016].

One example of the applications that require such high data rates is wireless transmission of high quality uncompressed video signal. Reconfigurable antennas can be one of the key elements to support high data rate communications. These antennas can significantly enhance radio system performance. Moreover, such antennas can be used in automotive radars, where it is necessary to steer the beam of the antenna and change its shape from omnidirectional to pencil beam. Reconfigurable antennas can also be used in satellite communications and airplane radars.

The history of reconfigurable antennas began in 1930's, when a two element antenna array was developed with the ability to steer nulls of the radiation pattern by using a phase changer in order to determine the direction of signal arriving [Friis1934], which then led to a steerable antenna [Friis1937]. Later, a multibeam antenna was proposed in [Simmons1966, Matthews1979].

These antennas can be classified into the following categories, by the type of reconfiguration:

- frequency reconfigurability – ability to cover different frequency bands;
- pattern reconfigurability – transformation from isotropic to very narrow antenna beam or pointing beam of the antennas to different directions;
- polarization reconfigurability – antenna elements can radiate waves of different polarizations;
- hybrid reconfigurability – which is the combination of previously mentioned three techniques.

Compared with conventional omnidirectional and fixed beam antennas, reconfigurable antennas can provide: larger coverage area, frequency reuse with fewer base stations, less probable co-channel interference, increased data rates, and, consequently, overall system capacity.

Recently, many different concepts have been developed in the reconfigurable antenna design to control the antenna bandwidth, resonant frequency, polarization, and radiation properties. Antennas using radio-frequency microelectromechanical systems, or RF MEMS, [Brown1998, Chiao1999, Rebeiz2003, Erdil2007, Kingsley2007, Civi2011], PIN-diodes [Nikolaou2006, Kim2008, De Luis2009, Di Palma2015], and varactors [Behdad2006, White2009, Cure2014] can be considered as electrically reconfigurable. PIN-diodes or varactors are faster comparing to RF MEMS. The switching time of the PIN diode is 1-100 ns, and for the RF MEMS it is in the range of 1-300 µs [Rebeiz2003], which can be too large in some applications. However, PIN-diodes have high losses and require rather high bias voltages for their operation. Optically reconfigurable antennas utilize photoconductive switching elements [Pringle2004, Tawk2010]. In Table 1 an overview of the technologies, which can be used in reconfigurable antenna structures, is presented [Hum2014].

Table 1. Technologies for the implementation of reconfigurable reflect arrays and reconfigurable array lens ("☺", "0", and "☹" symbols refer to good, neutral, and poor, respectively), based on [Hum2014].

Type	Technology	Reliability	Integration	D/A control	Complexity (cost)	Loss (microwave/THz)	Bias power consumption	Linearity	Switching time
Lumped elements	PIN diodes	☺	☹	D	☺	☹/☹	☹	0	☺
	Varactor diodes	☺	☹	A	☺	☹/☹	☺	☹	☺
	RF-MEMS	0	☺	D	☺	☺/0	☺	☺	0
Hybrid	Ferro-electric thin film	0	☺	A	0	0/☹	☺	0	☺
Tunable materials	Liquid crystal	0	0	A	0	☹/☺	0	0	☹
	Graphene	☹	☺	A	0	☹/☺	☺	☹	☺
	Photo-conductive	0	☹	A	0	☹/☹	☹	☹	☺
Mechanical	Fluidic	0	☹	A	0	0/☺	☺	0	☹
	Micromotors	☹	0	A	☹	☺	0	☺	☹

In this work, mechanically tunable antennas and antenna arrays using PIN-diode switches with the ability to reconfigure radiation characteristics are considered. Such antennas are of interest because of their ability to direct the beam towards the intended direction, which leads to power savings and improved signal to noise ratio. The antenna part of the thesis is dedicated to microfluidic antennas operating at 5.8 GHz and conformal antennas designed for the 60 GHz frequency range.

2.1. Antenna parameters

To describe antenna performance it is necessary to define various parameters and the relevant ones are described in this chapter. These parameters can be used for all antenna types independently on the antenna structure or operating frequency. First, the antenna radiation pattern is defined as a spatial distribution of a quantity that characterizes the electromagnetic field radiated by the antenna. The radiation pattern is defined in the far-field region and presented as a function of directional coordinates. The radiation pattern is usually characterized by the width of the main beam at half of its maximum power level, i.e. by the half power beamwidth (HPBW).

The antenna directivity $D(\theta, \varphi)$ is the ratio of the radiation intensity in a given direction from the antenna over the intensity averaged over all directions [IEEE1993]. The gain of the antenna $G(\theta, \varphi)$ combines the directivity and radiation efficiency of the antenna, which is the ratio between the radiated and accepted powers. The realized gain of the antenna comprises also mismatch losses [Balanis2005]. The directivity can be calculated as

$$D(\theta, \varphi) = D_\theta(\theta, \varphi) + D_\varphi(\theta, \varphi) \qquad (2.1)$$

while the partial directivities D_θ and D_φ are defined as

$$D_\theta = \frac{4\pi U_\theta(\theta, \varphi)}{(P_{\mathrm{rad}})_\theta + (P_{\mathrm{rad}})_\varphi} \qquad (2.2)$$

$$D_\varphi = \frac{4\pi U_\varphi(\theta, \varphi)}{(P_{\mathrm{rad}})_\theta + (P_{\mathrm{rad}})_\varphi} \qquad (2.3)$$

where U_θ and U_φ are the radiation intensities in a given direction contained in orthogonal θ and φ components; $(P_{\mathrm{rad}})_\theta$ and $(P_{\mathrm{rad}})_\varphi$ are the power in all directions contained in θ and φ components.

The realized gain of an antenna can be calculated as

$$G_{\mathrm{real}} = \eta_0\, D(\theta, \varphi) \qquad (2.4)$$

where η_0 is the total antenna efficiency.

Link budget calculation can be performed to estimate necessary antenna gains or the maximum distance between the antennas when the connection is possible. The frequency and distance dependence of the loss between two antennas in free space can be expressed by the Friis transmission equation:

$$\frac{P_r}{P_t} = G_t G_r \frac{1}{L_{FS}} \qquad (2.5)$$

where P_r is received power, P_t is the transmit power, G_t is the transmitting antenna gain, G_r is the receiving antenna gain, and L_{FS} is free space loss [Friis1946]. The free space loss is defined as:

$$\frac{1}{L_{FS}} = \left(\frac{\lambda}{4\pi R}\right)^2 \qquad (2.6)$$

where λ is the wavelength and R is the distance between the antennas. However, the atmospheric losses are not included in (2.5), which can have high impact on the propagation loss. Based on (2.5) and estimated atmospheric losses the necessary antenna gains can be calculated in the defined scenario if the distance between transmitter and receiver is known, assuming a pure line-of-sight (LOS) propagation channel.

In applications where the weight, cost, size, and performance are essential parameters, low profile antennas are often required. Microstrip antennas are good candidates since they can meet all the requirements mentioned above [Deschamps1953, Gutton1955, Munson1972, Howell1975, Pozar1992]. A microstrip antenna consists of a conductive patch and a ground plane

separated by a dielectric layer. Radiation from the patch is similar to the radiation from two slots, at the left and right edges of the patch, where the slot is the narrow gap between the patch and the ground plane. Due to the fringing effects, the electrical length is larger than the physical one. The increase in effective patch length and E-field of the patch antenna is illustrated in Fig. 2.2.

The radiation patch element can have various shapes, e.g. square, rectangular, circular, elliptical, etc. There are several methods to feed patch antennas: microstrip line, coaxial cable, aperture coupling, and proximity coupling. In this thesis, microstrip line feeding technique for the developed rectangular patch antenna arrays is used. Rectangular patch element dimensions can be calculated by the transmission-line model [Hammerstad1975, Bahl1980, Balanis2005]. The design procedure can be described as follows. First, we estimate the patch width

$$W = \frac{c}{2f_r} \sqrt{\frac{2}{\varepsilon_r+1}} \tag{2.7}$$

where c is the speed of light, f_r is the resonance frequency, ε_r is the relative permittivity. Next, the effective relative permittivity can be calculated as

$$\varepsilon_{reff} = \frac{\varepsilon_r+1}{2} + \frac{\varepsilon_r-1}{2}\left[1 + 12\frac{h}{W}\right]^{-1/2} \tag{2.8}$$

where h is the thickness of the substrate. After that the relation for the normalized extension of the length can be found:

$$\frac{\Delta L}{h} = 0.412\frac{(\varepsilon_{reff}+0.3)\left(\frac{W}{h}+0.264\right)}{(\varepsilon_{reff}-0.258)\left(\frac{W}{h}+0.8\right)} \tag{2.9}$$

The actual length of the patch is

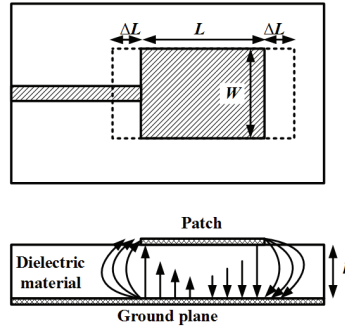$$L = \frac{c}{2f_r\sqrt{\varepsilon_{reff}}} - 2\Delta L. \tag{2.10}$$

Figure 2.2. Patch antenna, top and side views and the field distribution.

2.2. Millimeter-wave measurement setup

The measurement of the antenna radiation properties can be challenging, especially at mm-wave frequencies. Due to the small size of the mm-wave antennas, when high accuracy of the measurements is required, usually a connector can not be used, but it is possible to use probe measurement systems for far-field antenna pattern measurements [Ranvier2009, Zwick2004, Beer2010, Titz2012]. The antenna feeding can be designed, for example, for the ground-signal-ground (GSG) probe feed. If a microelectronic probe-feeding technique is used to contact the antenna, the use of mm-wave connectors can be avoided in the antenna measurements. This can be advantageous because the size of the connector is in order of wavelength at mm-wave frequencies and can disturb the antenna performance [Ranvier2009]. In addition, the antenna is probed at that part which will be connected later to the integrated circuit (IC) [Zwick2004].

In this work we have used quasi 3-dimensional measurement system [Titz2012] for characterizing the radiation properties of the developed antenna prototypes.The measurement system has an accuracy of ±0.8 dB at 60 GHz. The measurement system is presented in Figure 2.3 and it allows measuring the reflection coefficient of the antenna under test (AUT) and also the realized gain. The GSG-probe is used to feed the AUT, which is placed on a foam holder. The relative permittivity of the holder is close to 1 (ε_r = 1.01), which ensures that the radiation pattern under the antenna can also be measured. At the receiver side the harmonic mixer connected to the horn antenna is used. In order to measure the radiation pattern over the sphere two rotating arms are used. The measurements can be performed over 74% of the sphere. The only part where GSG-probe feeding cables are located, can not be measured. However, this part can be extracted from the simulations. The distance between the receiving horn antenna and AUT is 20 cm. The calibration procedure of the measurement system is described in [Ranvier2009]. The realized gain values can be computed after the measurements. The detailed description of the measurement system and measurement technique can be found in [Titz2012].
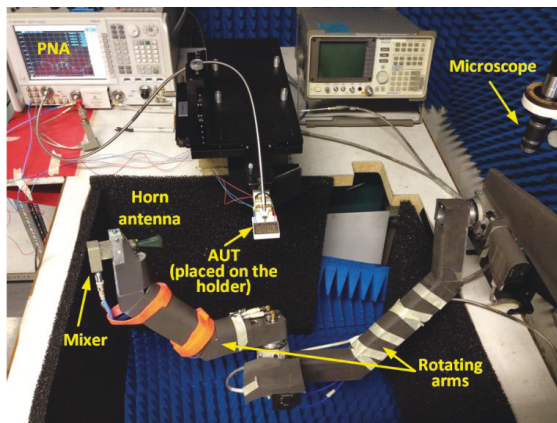

Figure 2.3. Antenna measurement system.

2.3. Reconfigurable antennas

The growing interest in flexible electronic devices requires stretchable and conformal antennas. The usage of standard metals such as gold or copper limits the development of versatile electronics. Elastic dielectric materials together with liquid metals enable bending and stretching of the developed antenna structure. Antenna structures with the use of liquid metals have been actively investigated in the last years. Usage of liquid metals such as mercury or gallium in the antenna structures has been studied in [Fayad2006]. One of the main advantages of these structures is their reconfigurability. The antenna can have any kind of shape and it can be changed using micro pumps in the structure [So2009, Dickey2013, Erdil2013]. This approach can be used to reconfigure the shape of the antenna and, consequently, control the radiation properties of the antenna. Beam steering can also be implemented by the usage of mechanically tunable antennas in a conformal installation. A cavity milled in the substrate defines the antenna shape. Injecting the liquid metal into one or more cavities forms the antenna configuration. These antennas can be dynamically adapted to the changes in the communication channel or in the system requirements.

Another interesting concept in reconfigurable antennas is the use of conformal antennas and arrays. According to the IEEE Standard Definition of Terms for Antennas: "conformal antenna is an antenna (an array) that conforms to a surface whose shape is determined by considerations other than electromagnetic; for example aerodynamic or hydrodynamic," [IEEE1993]. First investigations on conformal antenna arrays were done in 1930s [Chireix1936], where dipole elements formed an omnidirectional circular array. Also, a ring array of an infinite number of tangential dipoles, which can be azimuthally omnidirectional, was investigated in [Knudsen1953]. During the early years of World War II, a type of circularly disposed antenna array was developed, which received the name Wullenweber array [Joseffson2006]. Wullenweber technology was developed by the German navy communication research command for radio direction finding. During the Cold War similar systems were developed in different countries. Later, conformal microstrip antennas and microstrip antenna phased arrays providing omnidirectional coverage were studied [Munson1974]. Conformal antenna arrays can be placed on the several surfaces of an object [Vasylchenko2011] or on a continuous supporting structure [Liu2008, Cheng2013]. The azimuth coverage of antennas on continuous surfaces depends on the supporting object geometry [**II**]. If several antenna arrays are realized on the same printed circuit board (PCB) in a conformal installation with PIN-diodes, such an antenna structure can be used for beam steering or beam switching.

In the conventional planar antenna arrays, the beam can be steered in the range of maximum of ±70° without significant degradation of performance [Mailloux2005, Josefsson2006]. The scan loss in an ideal case is equal to $\cos(\theta_s)$, where θ_s is the scan angle, but in practice it is

$$scan\ loss = [\cos(\theta_s)]^\alpha \qquad (2.11)$$

where the exponent α may vary from 1 to 2 due to mutual coupling of array elements, impedance mismatch, resistive losses, etc. [Mailloux2005]. Figure 2.4 presents the scan loss dependance versus scanning angle, assuming that $\alpha = 1$. For the ideal case, the antenna gain decreases for about 4.7 dB for the 70° scan angle. At the same time, conformal antenna arrays can provide wider scanning angles with the same performance (without significant gain reduction), since the projection of the effective antenna area is larger.
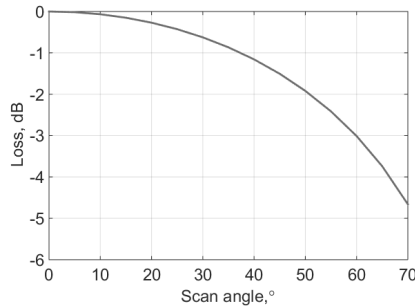

Figure 2.4. Scan loss versus scanning angle (mismatch losses are not taken into account).

2.4. Contributions of the thesis

2.4.1. Microfluidic antenna array

In [**I**], liquid metal patch antenna and reconfigurable antenna array operating at 5.8 GHz were developed and measured. Reconfigurability is achieved using liquid metal alloy which fills milled channels in the substrate of the antenna structure. Two antenna structures were designed using 3D full-wave electromagnetic fields simulator Ansoft HFSS™: a single patch antenna and a patch antenna array. The array is presented in Figure 2.5 and it is composed of 3 patch elements. First, the 2 mm deep channels for the liquid metal were milled in a 3.25 mm thick Rogers 5880 substrate. Next, the SMA connector was attached. The structure was covered with a thin film of polyethylene terephthalate (PET) material to prevent the liquid metal of going out from the structure. Then, gallium (Ga) alloy was injected into the milled channels.

The next step of the work was to perform radiation pattern measurements. The cylindrical measurement system in All-Russian Scientific Research Institute, Saint Petersburg, was used to measure the radiation performance of the developed antenna structures. Three cases have been simulated and measured: a single patch antenna, feeding one central patch antenna in the antenna array and feeding all three patches in the antenna array. Example of the measured radiation patterns can be seen in Figure 2.6. The measurements were not performed in an anechoic chamber environment. One of the appropriate techniques to compensate for reflections is to use an antenna pattern comparison technique (APC) [Appel-Hansen1973]. This technique was used to compensate the reflections for the central patch in the antenna array (Figure 2.6a).

28
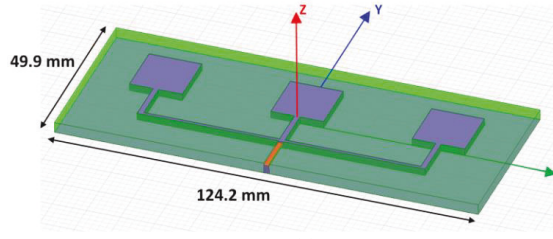
(a)

(b)

Figure 2.5. (a) Simulation model and (b) manufactured patch antenna array, from [**I**].
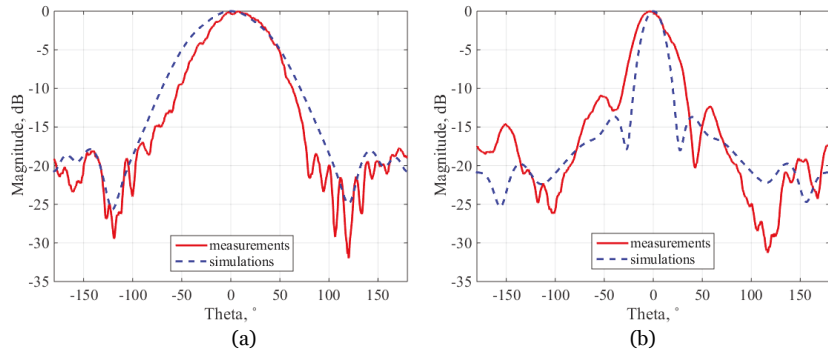

(a)

(b)

Figure 2.6. Normalized radiation pattern cuts, from [**I**] (a) feeding one central patch antenna in the array and (b) feeding all three patches in the antenna array.

In [**I**], the concept of reconfigurable antenna arrays using liquid metal alloy as the patch and strip material was studied. If micro-pumps, which can force the liquid metal to fill desired milled channels, are integrated into this antenna structure, the shape of the radiation element can be changed. The disadvantage of such a structure is low speed of changing the states. However, using properties of liquid metals can help to avoid the main disadvantage of mechanically-actuated reconfigurable antennas, for example, mechanical failures. Another advantage is that antenna arrays with liquid metal as a conductor on a flexible substrate can be deformable and mechanically tunable.

2.4.2. Conformal antenna arrays

Conformal antennas can be used in Wireless Local Area Networks to achieve high data rate communication. Microstrip antenna arrays are the most suitable antennas in conformal installations because of their low profile structure,

simple geometry and relatively inexpensive manufacturing. In [**II**], the conformal 4x4 patch antenna array has been developed for the frequency of 58.8 GHz. The optimized array pattern is placed on Taconic TLY-5 material substrate (ε_r = 2.2 and $\tan\delta$ = 0.0009 @ 10 GHz) with the thickness of 0.127 mm. The overall antenna size is 25x20 mm². The antenna array has been designed for short range communications, such as high definition video transmission in indoor environments. Publication [**II**] includes the performance measurement results for an antenna array placed on supporting structures with different radii (Figures 2.7, 2.8).
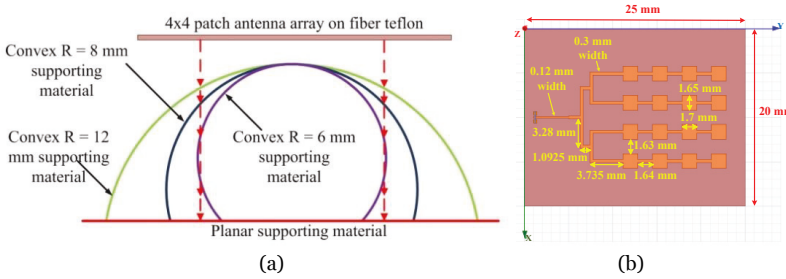

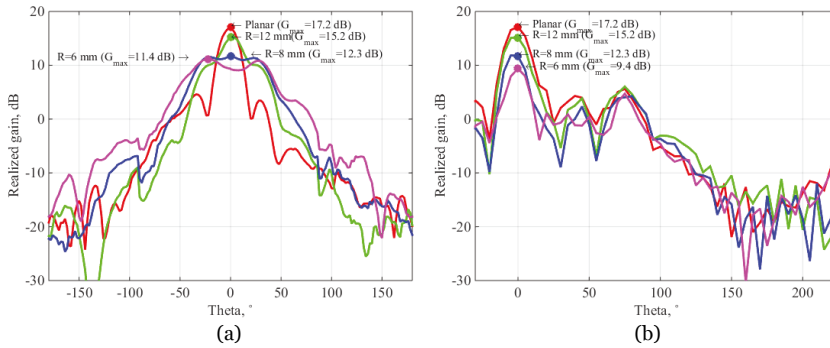**Figure 2.7**. (a) Schematic view of the studied cases and (b) antenna array structure from [**II**].

Figure 2.8. Measured total realized gain depending on the curvature radii in (a) XZ-plane and (b) YZ-plane, from [**II**].

Manufactured antenna prototypes were measured in La Turbie, France. The measurement system presented in [Titz2012] allows measuring fields on quasi-three dimensional sphere over the AUT. Realized gain values were measured versus frequency. In a planar case, the antenna array has a measured gain of 17.2 dB and it decreases to 11.4 dB if the antenna is placed on a convex supporting structure with the radius of 6 mm. Simultaneously, the HPBW of the antenna is enlarged up to 4 times, from 20° to 79°. It was shown that it was possible to obtain a wide azimuth coverage with the decreasing radii of the supporting cylinder. If several antennas are arranged on the cylinder surface, omni-directional coverage can be obtained with high gain values.

In [**III**], a beam switching antenna array is presented. Radiation properties for planar and conformal cases were studied. Such an antenna array can be integrated into smart watches for short distance high data rate communications. In particular, three 4x4 patch antenna arrays were designed

30

using a switching network. Each antenna array consists of 4 parallel connected series-fed linear arrays of 4 microstrip patches. The antenna array is optimized to operate at 59.9 GHz and the overall antenna size is 31x46.4 mm². The antenna consists of two metallic layers separated by a 0.127 mm thick Rogers RT/Duroid 5880 substrate with relative permittivity of 2.2 and the dielectric loss tangent of 0.0009 (@ 10 GHz). The top layer consist of 3 antenna arrays, DC pads for biasing the switch, and the switch mounting area. On the bottom layer there is a ground plane. To avoid using a multilayer structure for simplifying the manufacturing process, the biasing lines for the switch were also placed on the bottom layer, where the ground plane is partly etched. Blind via holes were drilled from the bottom to the top layer. The antenna array structure is presented in Figure 2.9. A single pole three throw (SP3T) switch was attached to the top layer of the PCB through copper pillar attachment. The feeding part of the antenna is designed for the GSG-probe.
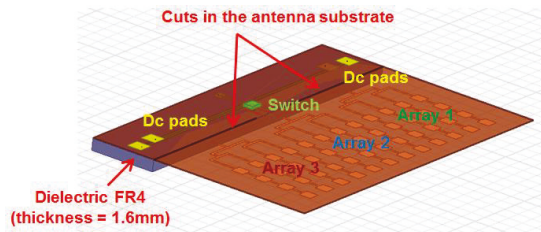

Figure 2.9. 3D view of the antenna structure.

Since the substrate is very thin and flexible, which can lead to breaking down the contacts between the switch and the PCB, FR-4 dielectric material layer was glued to the bottom layer of the antenna. One more reason is that the probing part of the antenna should be planar so that the antenna can be fed by a GSG-probe. For the conformal installation the antenna is placed on a cylinder, while the probing part remains planar. After antenna feeding pads, there is a transition to a microstrip and then back to a coplanar waveguide (CPW) for switch attachment (Figure 2.10a). It was necessary to make a CPW-microstrip-CPW transition, because of the dimensions between the switch pads, which did not allow to design a full CPW line from the probe to the switch. The transition was optimized in HFSS™ and simulated S-parameters are presented in Figure 2.10b. S_{11} and S_{22} are below -12 dB level over the frequency range from 57 to 63 GHz.

The losses in the switch were verified through indirect measurements for the planar antenna structure. The antenna structure without the switch was probed and the measured realized gain values were compared with the case when the antenna had a switch. The difference between these two measurements was 5.5 dB and could be caused by the mismatch in the switch connection and also insertion loss of the switch, the nominal value of which is 2.3 dB.

The realized gain values were measured for all three antennas in the planar case. Maximum values are 11.2 dBi for the first antenna array, 11.1 dBi for the second antenna array and 10.1 dBi for the third antenna array. Next, the

antenna was placed on a cylinder with the radius of 20 mm (Figure 2.11). Unfortunately, the bending of the antenna also affected the switch. Therefore, the radiation pattern of the central antenna array in a conformal installation could not be measured. The switch did not block the signal to the central antenna array and the feeding microstrip line for that antenna array was cut. Furthermore, the loss of the switch towards antenna 3 increased about 5 dB. The realized gain patterns of the side antenna arrays were measured and the results are presented in Figure 2.12. As can be seen, the scanning angles of the antenna are +34˚ and -32˚.

(a) (b)
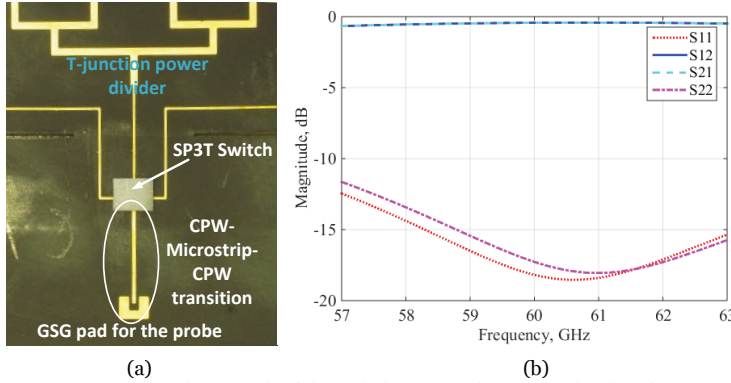
Figure 2.10. (a) Microphotograph of the switch-mounted area, (b) simulated S-parameters of the CPW-microstrip-CPW transition.

(a) (b)

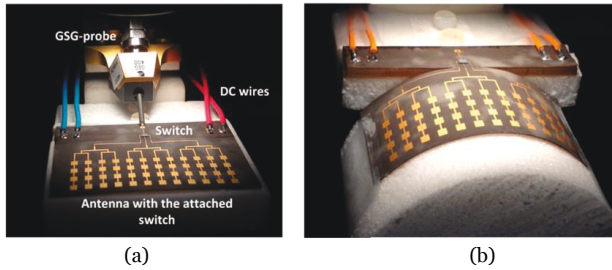**Figure 2.11**. Photographs of the developed antenna array from [**III**] (a) Planar antenna array, (b) Convex antenna array bent on the cylinder with R=20 mm.
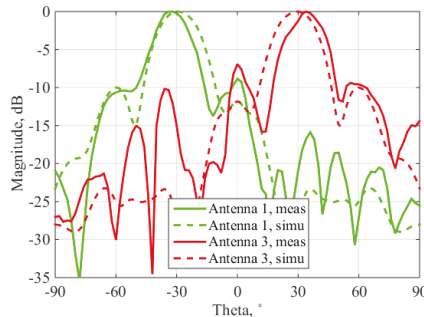

Figure 2.12. Measured normalized realized gain antenna radiation patterns, from [**III**].

The author has authored and co-authored also other related publications [Semkin2013a, Semkin2013b, Viikari2015, Ala-Laurinaho2015, Khairkar2016].

32

3. Radio wave propagation at mm-wave frequencies

Electromagnetic waves were described by J. C. Maxwell in the classical field theory [Maxwell1865] and, later, in 1880's they were discovered by Hertz, who was able to create an electromagnetic wave at about 50 MHz and to detect it [Hertz1887]. In 1890's researchers from different countries investigated the possibility to transmit information via radio waves. In 1895 A. Popov and G. Marconi presented their apparatuses which were able to transmit a radio signal. During the next year Marconi performed necessary experiments and in 1896 he applied for a patent. In 1901 Marconi succeeded in the first transatlantic radio transmission. In 1897 J. C. Bose presented his investigations of electromagnetic waves at cm- and mm- wavelengths [Emerson1998]. However, the mm-wave technology remained mainly unexplored until the middle of the 20th century. Only since 1960's mm-wave frequencies have been used by radio astronomers and by the military forces. In 1980's the development of millimeter wave integrated circuits created an opportunity to use mm-wave devices in the commercial applications. In 1990's automotive collision avoidance radar operating at 77 GHz was introduced. From that time mm-wave frequencies came to civil applications.

Nowadays, since the mobile traffic grows exponentially, the usage of mm-waves for data transmission can be used to improve the overall system capacity. Millimeter wave frequencies generally correspond to the radio spectrum from 30 GHz to 300 GHz, with the wavelength between ten and one millimeter. Compared to the signals at low frequencies which propagate for long distances and also through different objects, millimeter wave signals can propagate for only relatively short distances due to atmospheric attenuation and do not penetrate most solid materials. The atmospheric attenuation at these frequencies can be high. Millimeter waves are absorbed by the gases in the atmosphere, such as oxygen, water vapor, and others [FCC1997, Huang2011]. As can be seen in Figure 3.1, the attenuation at 60 GHz is more than 15 dB/km. However, mm-wave frequencies can provide wider spectrum and allow implementation of links in areas with a high number of users [FCC1997].
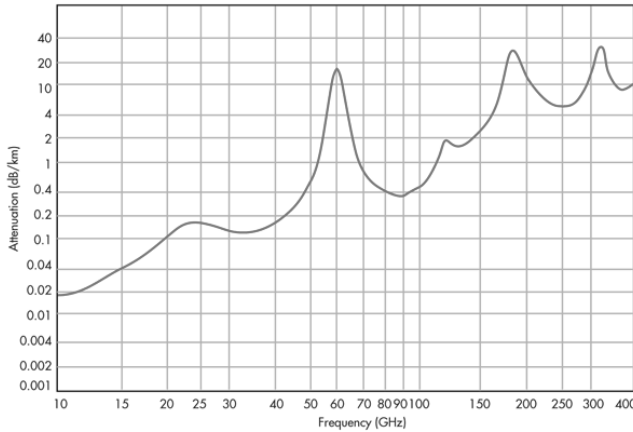
Figure 3.1. Atmospheric attenuation at mm-wave frequencies (at sea level, 20˚C temperature, 7.5 g/m³ of water content). Reproduced from [FCC1997].

The use of mm-wave frequencies for wireless communications has been supported by the standardization activities. The unlicensed frequency range from 57 to 66 GHz provides growing interest for wireless multi-gigabit communications for indoor environments [IEEE802.15.3c2009, IEEE802.11ad2012]. The frequency ranges from 71-76 GHz and 81-86 GHz (so called E-band) are used for fixed point-to-point radio communications [FCC2005, ETSI2006].

3.1. Ray-optical wave propagation

Electromagnetic theory development was possible due to the appearance of Maxwell's equations in 1864 [Maxwell1865]. Later, Sommerfeld [1911] linked these equations to the Geometrical Optics (GO) and this work was extended by Luneberg [1944] and Kline [1951], who showed that GO can be presented as an asymptotic solution of Maxwell's equations. The fields in GO are considered to travel along rays and can be derived geometrically. The GO can be used under the following assumptions [Hall1996]:

- all objects are large relatively to the wavelength;
- the surface is smooth on the wavelength scale;
- curvature radii of obstacles is large in wavelengths;
- the source and receiving points are separated by a large distance in wavelengths;
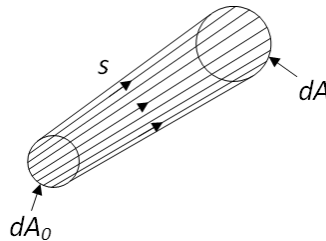- the distance between the nearest scatterers is large in wavelengths.

Figure 3.2. A ray tube, illustrating the intensity law of geometrical optics.

In the GO approximation, the energy is carried between two points in an isotropic medium using the conservation of energy flux in a tube of rays. A ray tube is a tube the lateral surface of which is formed by a set of rays, and the bases are two wave front sections (Figure 3.2). In the ray tube the energy flux remains constant and the power density (or intensity) is inversely proportional to the cross-section of the ray tube

$$U_0 dA_0 = U dA, \tag{3.1}$$

where U_0, U are the radiation power densities and dA_0, dA are the cross section areas of the tube separated by distance s. Therefore, the power carried by a ray attenuates even in lossless media due to the enlarging of the ray tube cross-section.
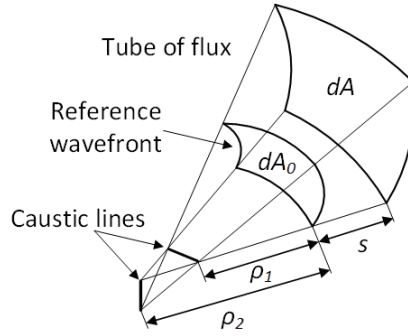

Figure 3.3. Astigmatic tube of rays.

It is necessary to define an astigmatic tube of rays, which is a more general configuration of ray tubes, where the rays in the tube are perpendicular to the wavefront and not focused at one point, but pass through two lines called caustics. For an astigmatic tube of rays, presented in Fig. 3.3, the complex electric field amplitude, including phase and polarization, can be found as [Saez de Adana2011]

$$\vec{E}(s) = E(0)\sqrt{\frac{\rho_1 \rho_2}{(\rho_1+s)(\rho_2+s)}} e^{-j\beta s}, \tag{3.2}$$

where $E(0)$ is the electric field at the reference point, $\beta = \frac{2\pi}{\lambda}$ is the propagation constant in free space, ρ_1 and ρ_2 are the curvature radii of the wave front at the reference point. The GO field in caustics is infinite because an infinite number of rays pass through them. There are three possible cases. First, if the two caustics deteriorate into a single point, then the wave front becomes spherical. Second, if one of the two caustics is formed at an infinite distance the wave front is cylindrical. Third, if both caustics are formed at an infinite distance then there is a plane wave.

As it is mentioned above, there is a significant limitation for the GO, when applied to radio-frequency problems; it is not possible to define the field in the shadow areas and at the shadow boundaries. The solution was proposed by

Keller [1962], who introduced diffracted rays, which allowed predicting the high-frequency field on the edges of objects. From that time an extension of GO, which was called Geometrical Theory of Diffraction (GTD), appeared. Later, the theory was further developed, because the original GTD proposed by Keller contained some problems, such as infinite diffracted field outside the shadow and reflection boundaries. This lead to the appearance of the Uniform Theory of Diffraction [Kouyoumjian1974].

3.2. Propagation mechanisms

Radio waves propagate in space according to several interaction mechanisms with the surrounding objects: free space propagation, reflection, transmission, diffraction, and scattering, as shown in Figure 3.4. Human blockage can also have a high impact on the radio wave propagation at mm-wave frequencies.
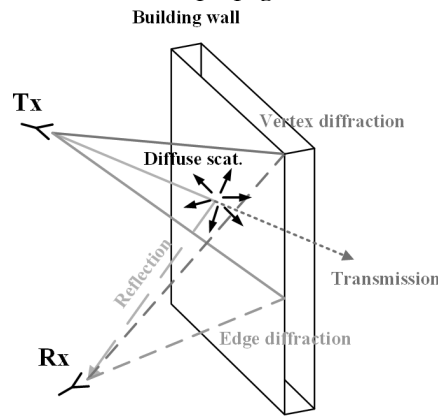

Figure 3.4. Possible propagation mechanisms by rays facing the building wall. Adopted from [Degli-Esposti2014].

3.2.1. Free-space propagation

The waves propagating from the transmitter (Tx) to the receiver (Rx) without any obstacles, and when there is only a line-of-sight connection, can be described by the free space propagation model [Friis1946]. The frequency and distance dependence of the loss between two antennas in free space can be expressed by Friis' law (2.5). The free space loss factor is defined as in (2.6).

3.2.2. Ray reflection and transmission

Electromagnetic waves are often reflected at one or more objects before arriving at the receiver. Reflection is one of the dominant propagation mechanisms. Usually, if the interaction objects have smooth surfaces and are larger than the wavelength, only transmission and specular reflection take place (Fig. 3.5). When a ray impinges on a plane surface, the incident field is split into an incident, a reflected, and a transmitted one. The incident ray trajectory is modified according to Snell's law, where the angle of incidence (θ_i) is equal to the reflection angle (θ_r).
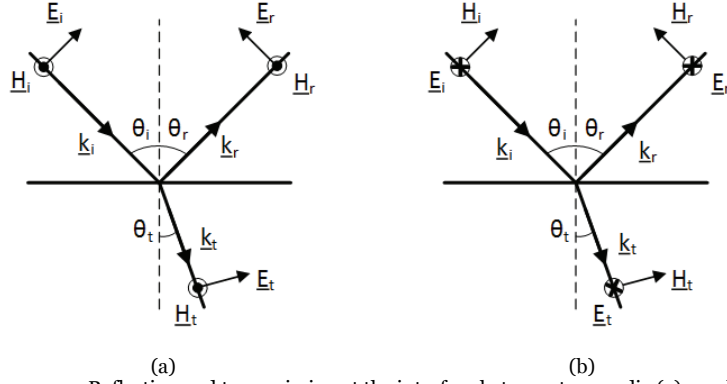
36

(a)   (b)

Figure 3.5. Reflection and transmission at the interface between two media (a) parallel polarization, (b) perpendicular polarization.

The field amplitude and phase changes at the interaction point can be calculated according to proper Fresnel's reflection coefficients, which can be found, e.g., in [Mittra2014].

3.2.3. Scattering from rough surfaces

For a smooth surface, the total energy of a ray is reflected in the specular direction, as it was shown in the previous section. However, in the real cases, some portion of energy is scattered in all directions due to the roughness of the surface. This mechanism is very relevant at mm-wave frequencies, since roughness of a surface can be comparable with the wavelength. Scattering effect can have a large impact on the ray tracing simulations in urban environments since the surfaces of buildings are not ideal. There are two main theories which describe the scattering mechanism: Kirchhoff's theory and the perturbation theory. For the surface roughness estimation Kirchhoff's theory requires that the probability density function of surface height is known. It assumes that the height variations are small enough not to influence the nearest scattering points. If this condition is fulfilled, the specular reflected ray will be attenuated by a certain value. The decrease of the power can be described by the effective reflection coefficient [Molisch2011]:

$$\rho_{\text{rough}} = \rho_{\text{smooth}} e^{-2(\beta \sigma \sin \theta_i)^2} \qquad (3.3)$$

where ρ_{rough} is the effective reflection coefficient, ρ_{smooth} is the reflection coefficient from the smooth surface, β is the propagation constant, σ is the standard deviation of the height distribution, and θ_i is the angle of incidence. However, the Kirchhoff theory is limited and cannot be used for small angles of incidence, since the height variation in a surface roughness becomes significant.

The perturbation theory, in addition to the probability density function, utilizes the spatial correlation function. In this case it is not probable that a shadowing region will appear. The effect of the surface roughness on the

specularly reflected ray can be described by a complex dielectric constant, which influences the reflection coefficient. More detailed description and formulas for the complex dielectric constant can be found in [Vaughan2003].

Different statistical scattering models were proposed by Didascalou [2003], Kloch [1997], Degli-Esposti [1999]. However, it is necessary to validate proposed scattering models by measurements. In [Degli-Esposti2007], scattering from different types of walls was measured and modeled at 1296 MHz, and in [Al-Nuaimi1994], a measurement campaign was conducted at 11.2 GHz to estimate the scattering effects from real buildings. Langen, *et. al.* [1994] performed amplitude measurements of a signal to define the scattering properties at 60 GHz. In [**V**], a wideband channel measurement system was used to define the multipath components from the LOS connection and the scattering patterns were measured from different observation angles at E-band. In contrast with Langen's [1994] work, not only amplitude measurements have been performed, but also phase information has been acquired.

3.2.4. Diffraction and human blockage models

The main limitation of the GO is that only direct and reflected fields can be predicted. In order to predict the electromagnetic field in the shadow regions, the extension of the GO, called geometrical theory of diffraction (GTD), should be used, which takes into account diffraction effects. According to the GTD, the incident ray causes an infinite number of diffracted rays, which are placed on Keller's cone, Figure 3.6. However, the GTD exhibits singularities at shadow boundaries and caustics. A uniform asymptotic method, i.e. uniform theory of diffraction (UTD), was proposed by Kouyoumjian [1974] to calculate the fields in all regions. The UTD includes Fresnel integrals in the diffraction coefficient and gives an accurate result close to the boundaries [Mittra2014].
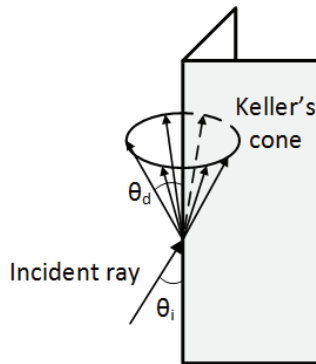

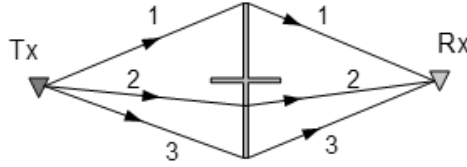**Figure 3.6**. Diffracted field on the edge.

Figure 3.7. Top view of the MKE diffraction model, rays 1 and 3 represent diffraction over the human body, and ray 2 represents diffraction over the head.

Different diffraction models of human bodies have been studied [Ghaddar2007, Gustafson2012]. In this thesis, we have used multiple knife edge (MKE) diffraction model for human blockage developed by Jacob [2011, 2013] in the ray tracing simulations [**IV**]. This human blockage model was extended from a double vertical knife-edge diffraction model developed by Kunisch [2008]. The extended model includes an additional plane which is parallel to the body axis. This improvement is necessary, since in the original model the diffracted rays are not taken into account if the person movement is parallel to the propagating ray. In addition, the MKE diffraction model takes into account diffraction over the human head (Figure 3.7).

3.3. Characterization of radio wave propagation at mm-wave frequencies

3.3.1. Ray tracing techniques

Ray-optical modeling algorithms can be divided into two categories: the image method (IM) and the shooting-and-bouncing ray (SBR) method [Mittra2014]. Usually, algorithms based on IM are called Ray Tracing (RT) and algorithms based on SBR method are called Ray Launching (RL). Ray Tracing is a technique for generating an image of a source by calculating the paths taken by rays of light entering the observer's eye at different angles. This technique is widely used not only in computer graphics, but also in radio wave propagation studies [Döttling1997a, Degli-Esposti2014, Fugen2007, Fuschini2008, Rautiainen2007]. If the wavelength is smaller than the surrounding objects, electromagnetic waves can be approximated by rays for which the geometrical optics rules are valid. Deterministic propagation models based on Geometrical Optics and Uniform Theory of Diffraction can provide reliable estimations of radio wave propagation in a specific environment [McKown1991].

Another method is the shooting-and-bouncing ray (SBR) method, or so-called ray launching, which also belongs to the group of deterministic models and can be used for radio wave propagation modelling [Kipp2004, Sato2005, Rose2014]. In the SBR method the rays are launched from a transmitter towards all directions in order to cover the angular space around the source. When a ray hits an object, it is split into transmitted and reflected ones. The relationship between the angles of incidence and refraction is calculated by Snell's law. In comparison, the IM cannot use Snell's law because the Tx and

Rx positions are fixed. The diffracted field is calculated on the edges and vertexes of the objects. The SBR is a direct method and it does not depend on the observation point position of the Rx antenna. The rays that reach the observation point contribute to the total electromagnetic field [Mittra2014]. Ray Launching method can be more suitable for planning the wireless networks since it is computationally more efficient than Ray Tracing [Gschwendtner1995]. The SBR method is preferable for the use in complex environments, since the IM can be computationally inefficient when there are higher order reflections and diffractions, especially in 3D models.

There are also other ray tracing techniques, developed from the IM/SBR method or their combination [Liang1997, Iskander2001, Mohtashami2010, Liu2012], however, they are not in the scope of this thesis.

3.3.2. Photogrammetry and its applicability for ray launching simulations

Since wireless radio links can be strongly influenced by propagation effects, it is necessary to know the detailed geometry of the environment. This is especially true at mm-wave frequencies when all the details of the object geometry can influence the propagation characteristics. A ray tracing software requires as input the object geometry. Considering urban scenarios with a lot of small objects like details of the facades of the buildings, traffic lights/signs etc., a detailed geometry description of the environment is needed in order to get reliable results for radio wave propagation prediction.

Photogrammetry is a technical method to reconstruct 3D objects from two or more planar images [Kraus2007]. The concept of photogrammetry goes back to 15th century, when Leonardo da Vinci developed the concept of perspective and projective geometry. Here we will consider only digital photogrammetry which is a relatively new field.

Close range photogrammetry is a technique for accurately measuring objects directly from photographs or digital images captured with a camera at a close range. Multiple overlapping images taken from different perspectives, produce measurements that can be used to create accurate 3D models of the objects. Nowadays, close range photogrammetry is used in many areas: mapping, agriculture, environmental monitoring, inspection of buildings and bridges, real estate, construction, and many others. Close range photogrammetry models can be obtained by terrestrial images, aerial images, or by the combination of these types of images.

There are some other options to obtain 3D data of the environment. One option can be an Open Street Map (OSM) data [Nuckelt2013], however the OSM models do not contain all details of the building geometry and do not take into account small objects placed on the facades and rooftops of buildings. Another method to obtain data about the environment can be the Light Identification Detection And Ranging (LIDAR) technology [NOAA2012]. However, photogrammetry can have the same accuracy as laser scanning and it can be more cost effective compared to the LIDAR technology [Leberl2010, Hyyppä2011, PIX4D2014]. Moreover, in some scenarios it is difficult to use LIDAR, for example if information about rooftops of a group of buildings is

necessary. Usage of small and ultra-small unmanned aerial vehicles (UAVs), or so-called drones, equipped with cameras, together with photogrammetry software can solve this problem. There are some published works where the authors combine LIDAR technology and UAV in order to obtain 3D models of environments [Pop2007]. In contrast with the UAV using conventional photo cameras, this technology is more expensive and can be more dangerous if the survey is done in a densely populated area, since the weight of the UAV with LIDAR is high. Another issue is that using LIDAR on the UAVs will require more time to obtain the data because the vertical field of view is usually limited in the LIDAR devices.

In our research work, we have used a drone with a wide angle field-of-view camera to build high accurate 3D models of outdoor environment [**VII**]. This model can be used in radio wave propagation simulation which will help to optimize allocation of mobile network infrastructures. Based on a 3D point cloud, being the output of the photogrammetry software, a 3D mesh model can be generated. This model can be used in radio wave propagation modeling using IM or SBR methods.

3.3.3. Channel modeling of an urban street canyon

The E-band, which consists of 71-76 GHz and 81-86 GHz sub-bands, is widely used in high data rate point-to-point communications. The available 10 GHz of spectrum allows transmitting several gigabits of data per second. Such radio links can be installed in densely populated urban areas to provide high data rate backhaul communications. However, the surrounding environment can have a high impact on the communication channel. It is especially true for urban scenarios, where there are a lot of objects, like traffic lights, signs, etc., which provide scattered multipath components. One approach to model street canyons is ray tracing simulations [Hur2016, Döttling1997b]. But considering delay domain properties there can be a significant difference between measurements and simulations. One reason can be that the Ray Tracing underestimates power and the number of multipath components. For this reason measurement-based stochastic channel models can be used to study the E-band propagation. In [Liberty1996], a geometrically based model for single bounce multipath components in line-of-sight (LOS) radio wave propagation channels was developed. However, this model is not designed for urban street canyons, where various small objects should be taken into account. In [Kyrö2012], a 2D single bounce channel model based on the delay domain was developed for a street canyon scenario. In this model, random scatterers are taken into account. The location of the scatterers is defined by an ellipse, the diameter of which is limited to the street width. The excess delay and received power of multipath components can be defined by this model. Nevertheless, this model needs refinement in terms of an extension to a 3D model and this extension will be described in the following section.

3.4. Contributions of the thesis

The main research foci of this work, related to radio wave propagation at mm-wave frequencies, are:

- development of a method for estimation of the optimum antenna configurations supported by ray tracing simulations;
- empirical characterization of scattering patterns at mm-wave frequencies;
- extension of the developed 2D channel model in [Kyrö2012] to a 3D model based on the angular distribution of scatterers in an urban street canyon;
- characterization of radio links at mm-wave frequencies using highly accurate photogrammetry models.

3.4.1. Estimation of optimum antenna configurations

In [IV], we have performed ray tracing simulations in realistic scenarios using human blockage models, described briefly above, to estimate suitable antenna configurations in a conference room scenario. The ray tracing software was developed in Technische Universität Braunschweig and a comprehensive description of the RT software can be found in [Priebe2012]. In the RT simulations we have used planar and conformal antenna arrays developed in [Semkin2013a] and [II]. A conformal antenna with one fixed beam was used as a receiver. For the Tx side, we have used different numbers of antennas each pointing to different direction, with the ability to switch the beam between the antennas, placed on the faces of the polyhedron surface. To evaluate realistic conditions for the conference room scenario, one to ten people randomly walking in the room were added to the ray tracing model. The movement of the person was modeled with a random walk algorithm, where MKE diffraction model with the dimensions 170x45x40 cm^3 was used. The walking speed was set to 1 m/s and the step length was defined to be 60 cm. In Fig. 3.8, the conference room scenario with the antenna radiation patterns (only one position for the Tx is shown), rays, and one person's moving trajectory are presented. The main idea was to evaluate the necessary number of antenna arrays at the Tx side in order to maintain a stable communication between Tx and Rx if the LOS is blocked by the human being. In these simulations, beam switching technique is used to reconfigure the Tx antenna radiation properties so that the strongest multipath component is utilized for the communication. We considered 180° and 360° coverage by the Tx antenna arrays with different beam switching steps, i.e. 30°, 15° and 5°. In Figure 3.9, as an example, a comparison of the received power levels for an LOS connection and the connection using reflected paths, when 10 people are randomly walking in the room, is presented. The minimum required power level is -63 dBm level [IEEE802.11ad2012]. Therefore, blockage should be avoided. It is obvious that beam steering of the Tx antenna leads to the power increase for most of the cases.
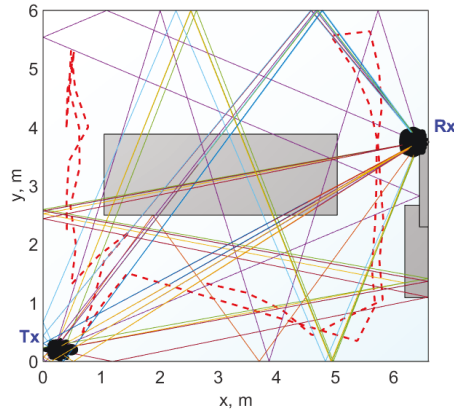
Figure 3.8. Top view of the conference room used in ray tracing simulations; planar and conformal antenna arrays are used as a transmitting and receiving antennas (solid lines represent rays, dash line represents trajectory of a person's movement).
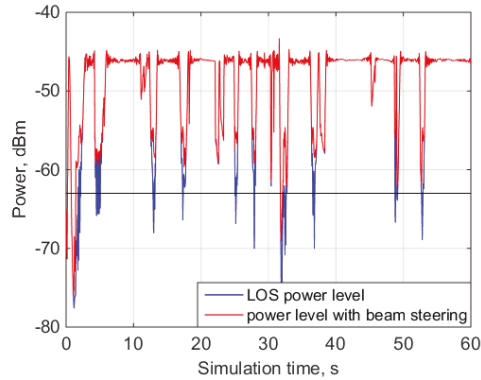

Figure 3.9. Comparison of the power levels for 360° coverage with 5° beam steering step for one of the Tx positions (blue line: LOS connection, red line: reflected paths by beam steering, black line: the -63 dBm level); from [**IV**].

(a)   (b)

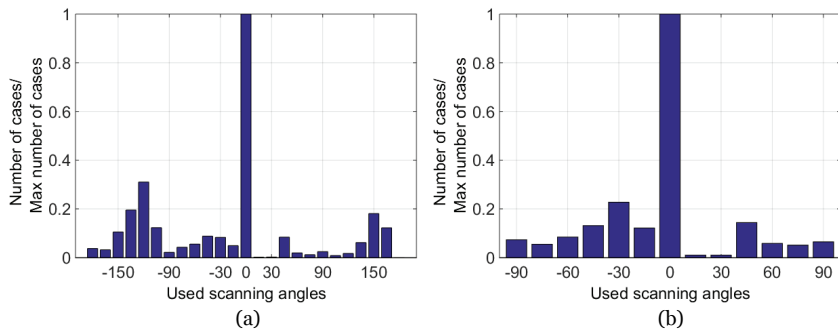**Figure 3.10**. An example of used scanning angles by Tx antenna array network (a) 360° coverage with 15° step (b) 180° coverage with 15° step; from [**IV**].

Analyzing the statistical distribution of the angles used in the stable communication (one of the examples with two different antenna configurations is presented in Figure 3.10) and by probability to overcome the
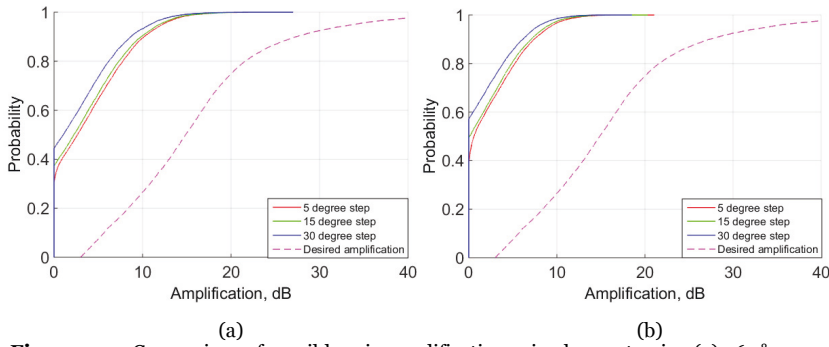
(a)   (b)

Figure 3.11. Comparison of possible gain amplification using beam steering (a) 360˚ coverage (b) 180˚ coverage; from [**IV**].

human blockage of the signal (Figure 3.11), the optimum antenna configuration was verified for this scenario.

Figure 3.11 shows the probability of the power amplification which can be achieved to compensate the losses for different cases. As a reference, the figure includes desired amplification, when all losses would be compensated. It was shown that an antenna array configuration with the 180˚ coverage and the 15˚ angular step can be used in this scenario since such a structure is less complex and there is only minor difference the with 360˚ coverage case. Similarly, RT simulations were performed with Gaussian antenna patterns. The main idea was to show that estimation of optimum antenna configurations in a specific scenario can be done by approximating antenna radiation patterns with Gaussian shaped beam patterns. Hence, if the antenna requirements are known, such a method can be used to verify if this antenna is suitable for the usage in a particular environment.

3.4.2. Characterization of scattering patterns at mm-wave frequencies

In [**V**], the scattering patterns were characterized by measurements in the 69-74 GHz frequency range for two different materials, i.e. brick and glass walls. These are typical materials for large number of buildigs. A wideband measurement system, which allowed obtaining phase information, was utilized to measure the channel transfer functions. Multipath components were distinguished from the direct LOS path and the scattering patterns were measured at different illumination angles. The reflected and scattered signals were measured by illuminating the wall from one angle and receiving signal from several different directions (Figure 3.12). Figure 3.13 shows the measured LOS and reflected path. The reflected path has a tail in time domain which shows that the reflection did not happen from a single point but from larger area. The scattering patterns could be measured since the distance between Rx and Tx via reflection from the wall is always 6 m. This corresponds to 20 ns delay in the time domain. The received power level for 20 ns delay time was used to plot scattering patterns from the brick and glass wall.
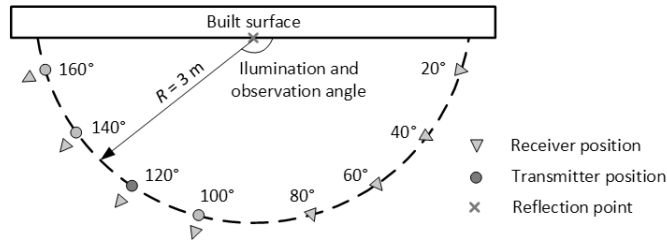
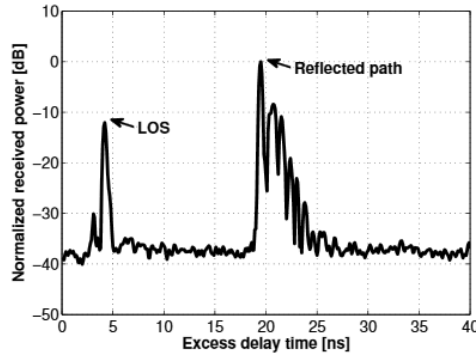**Figure 3.12**. Tx and Rx antenna location during the measurements.

Figure 3.13. An example of the averaged power delay profile from the brick wall measurements when the Tx antenna is pointing to the wall; from [**V**].
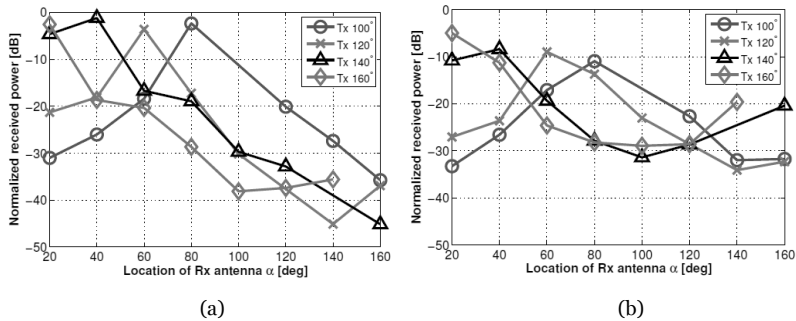

Figure 3.14. The scattering patterns of (a) the brick wall, (b) the glass wall; from [**V**].

It was found that the reflection loss at the mirror reflection angles is 1-4 dB for the brick wall and the losses increase up to 45 dB as a function of the observation angle. For the glass wall the reflection loss is 5-10 dB for the mirror angles. It is larger in comparison with the brick wall because the signal partly penetrates through the glass. The losses increase up to 34 dB with changing the illumination angle. The scattering patterns are presented in Figure 3.14. Obtained results can be utilized in radio wave propagation modeling in urban environments with geometry-based stochastic models.

3.4.3. E-band propagation channel measurements

E-band radio wave propagation in a street canyon scenario is characterized in [**VI**]. An angular distribution of scatterers was measured in Helsinki

downtown. Based on the angular spreads an existing 2D channel model developed by Kyrö [2012] and described later by Räisänen [2013], was extended to a 3D channel model. First, the geometrical parameters should be included into the channel model: distance between Rx and Tx; the street width and height; the number of multipath components; the deviation of scatterer locations; and the reflection loss. After the parameters are defined, the power of the LOS component is calculated. The ellipsoid is defined according to the distance between the Rx and Tx so that their positions are located in the foci. Next, the location of each scatterer is defined (Figure 3.15) and the direction of arrival and direction of departure are calculated according to the scatterer locations. After these steps have been performed, the power angular spectrum can be calculated. The results are presented in Figure 3.16. The developed 3D channel model can be used to calculate realistic values of the power angular spectrum for the street canyon scenario.
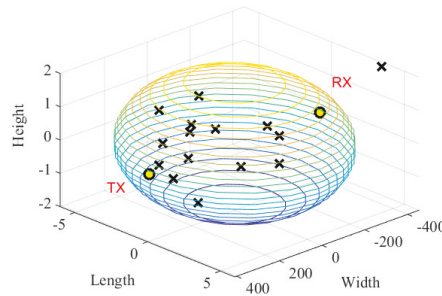
Figure 3.15. Location of scatterers and the ellipsoid which represents street canyon scenario.
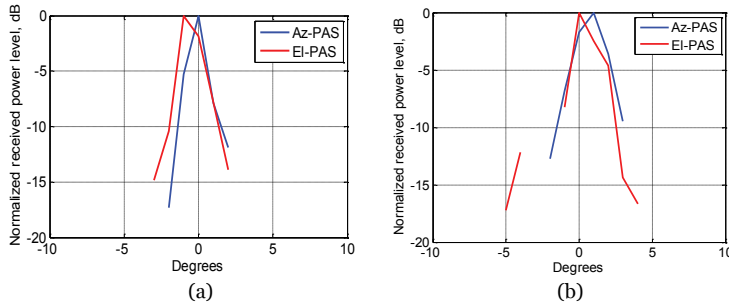
Figure 3.16. Power angular spectrum (PAS) for 800 m distance: (a) measured and (b) simulated. Reproduced from [**VI**].

3.4.4. Characterization of radio links using 3D models

In order to deploy effectively high data rate wireless communications in urban environments, the information about the radio wave propagation channel is essential. In [**VII**], a measurement campaign has been carried out in order to evaluate the propagation effects in the radio channel on the rooftop of the buildings. The measurements were performed in 59-63 GHz frequency range for 6 different locations of the Tx antenna, while the position of the Rx was fixed. Later, the measurement results were compared with the simulation

results in terms of the power delay profile. Two 3D models were used in SBR simulations: 1) simple geometrical and 2) highly accurate close range photogrammetry model. The measured and simulated power delay profiles were compared to estimate if highly accurate 3D models can be beneficial in radio wave propagation planning instead of using simple geometrical models at high frequencies. In the simple geometrical model, the environment for the simulations is constructed from simple geometrical figures. Close range photogrammetry model is formed from the high resolution images obtained by a drone, which is shown in Figure 3.17. Total captured area is 15600 m². These images were processed by the photogrammetry software and a 3D point cloud of the environment was obtained. Based on the received point cloud, all objects were measured and a 3D mesh model was created in the computer aided design program. Both 3D models were exported into the Remcom Wireless InSite software (Figure 3.18.).

Figure 3.17. Photo of the drone, used for obtaining the photographs for the 3D model.

During the measurements, power delay profile (PDP) was measured for 360° rotation of the Rx antenna, the position of which was fixed. The measurements were performed for 6 different positions on the rooftop. After that the measured PDPs were averaged and the same was done in simulations. An example of an averaged PDPs is presented in Figure 3.19. As can be seen, the simulation results using the highly accurate photogrammetry model are generally more accurate than using simple models. Simulated results of the PDP for simple geometrical model underestimate the power almost for the whole simulated delay range. This happens because there are many small objects, in terms of the overall area size, which affect the PDP characteristics. The PDP simulated with the photogrammetry model agrees better with the measured results. As a conclusion, in this work we have verified how a detailed elaboration of the environment can affect predictions of the propagation characteristics at mm-wave frequencies.
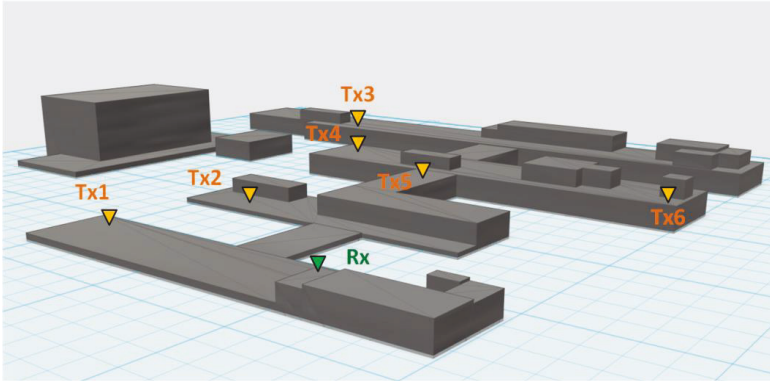
(a)
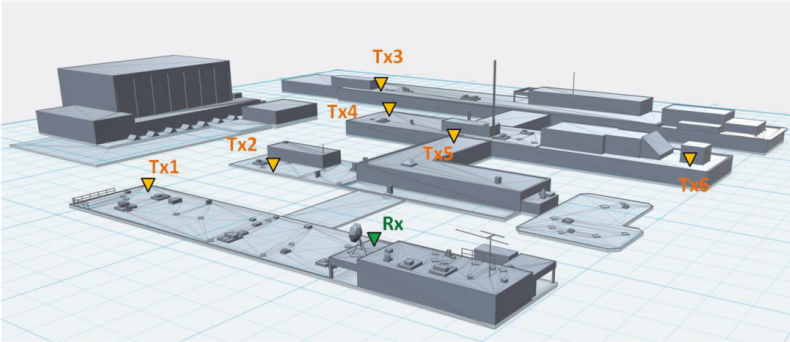
(b)

Figure 3.18. 3D models used in SBR simulations: (a) simple geometrical model and (b) close range photogrammetry model.
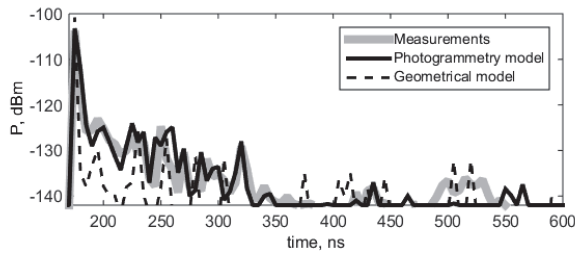

Figure 3.19. An example of averaged power delay profile for the first Tx position (53 m LOS distance).

4. Summary of publications

Reconfigurable antennas at micro- and mm-wave frequencies

In [**I**], mechanically reconfigurable antennas with the ability to change their radiation properties are studied. A microfluidic patch antenna and an antenna array designed at 5.8 GHz for utilization in the wireless local area network applications are presented. Liquid metal gallium is used to fill the milled channels in the antenna substrate in order to change physical pattern of the radiating element. Designed antennas have good matching properties and relatively symmetrical radiation patterns.

Investigation of the performance of conformal antenna arrays placed on cylindrical structures with different radii is presented in [**II**]. The antenna array is fabricated on polytetrafluoroethylene (PTFE) substrate. Measurement and simulation results for both planar and conformal antenna arrays show rather good agreement. It is shown that the gain of the antenna decreases while the HPBW increases with the smaller radii of the supporting structure. A beam switching conformal antenna is presented in [**III**]. The antenna is designed to operate at 59.9 GHz and the performance of the built prototype is compared with the simulation results. For the beam switching implementation a single pole three throw (SP3T) switch is attached to the antenna structure using copper pillar attachment. Beam switching is demonstrated for the conformal antenna placed on the cylinder with 20 mm radius and scanning angles of -32°/+34° are obtained. Such antennas can be integrated, for example, into smart watches to support high data rate communications for short distances.

Radio wave propagation at millimeter-wave frequencies

In [**IV**], an estimation of optimum antenna configurations supported by ray tracing simulations is presented. Developed antenna arrays in planar and conformal installations are used at the receiver and transmitter side. The influence of human blockage on the propagation channel in a conference room is investigated by simulations for different number of persons randomly walking in the room. Moreover, it is shown that antenna radiation patterns can be approximated with Gaussian beams. By the obtained results the best antenna configuration for the specific environment can be estimated.

In order to empirically characterize reflection and scattering properties of built surfaces, measurement results are analyzed in [**V**]. The measurements are performed in the 69-74 GHz frequency range and the reflected and scattered multipath components are identified from the measured power delay profiles.

A 2D stochastic geometrical single-bounce channel model for urban street canyons based on angular-domain measurement results has been extended to a 3D channel model in [**VI**]. The measured power angular spectra are in a good agreement with the results provided by simulations with the developed 3D channel model.

In [**VII**], the influence of small environmental structure details on the propagation characteristics is studied. A comparison between measurement and simulation results at 60 GHz is provided by performing shooting-and-bouncing ray simulations for the rooftop-to-rooftop scenario using 3D environment models with different detalization. In addition, it is shown that the photogrammetry technique can be a beneficial method in obtaining higly accurate 3D models for further use in the ray tracing or ray launching simulations.

5. Conclusions and future work

In this thesis, reconfigurable antennas operating at micro- and mm-wave frequencies, and peculiarities of the radio wave propagation in the mm-wave frequency range have been studied. The first part of the work deals with the mechanically and electrically reconfigurable antennas with the ability to change their radiation properties, i.e., the HPBW of the radiation pattern and main lobe direction. Microfluidic technology is investigated, and it is shown that liquid metall alloys are good candiates in the reconfigurable antenna design. However, this technology can be utilized only if the time spent in changing the states is not a critical factor.

Next, the performance of the conformal antenna arrays is investigated. The characteristics of the developed antenna prototypes are validated by the measurements using a probe fed antenna measurement system. The radiation patterns of the antenna can be changed by placing the antenna on objects with different curvature radii. Based on these results, several antenna arrays have been designed together with the switching network. Conformal antenna structures using beam switching technology can be beneficial for high-capacity communication systems. If the line-of-sight (LOS) link is blocked, the main beam direction can be controlled in order to get the highest level of the received signal through a reflection. Future work may contain studies on the antenna packaging and integration of the conformal antennas with the devices, such as smart watches, mobile phones, or radio access points. Conformal antenna design may be improved as well, by characterizing different substrate materials at mm-wave frequencies.

The second part of the thesis is addressed to the following problems: how to optimize antenna design for a specifc environment and how to deploy mobile networks efficiently taking into account the peculiarities of radio wave propagation in the mm-wave frequency range. Supported by ray tracing simulations it is shown that optimum antenna configurations can be designed for a specific environment. If the requirements for the antenna design are known, ray tracing software and human blockage models can be used to verify if stable connection is possible using developed antenna structures.

The long range channel in an urban environment has been characterized through the measurements. The measurement results have been utilized to create a 3D propagation model for a street canyon scenario. The model can be used to calculate realistic power angular spectra in the azimuth and elevation planes.

The influence of small structural details of the environment on the propagation characteristics at 60 GHz has been studied. Higly accurate and simple geometrical models have been obtained for ray launching simulations and the measured delay domain multipath characteristics have been compared with the simulated ones. It is found that the usage of a highly accurate model obtained with photogrammetric technique provides in the ray launching simulations more precise power delay profile prediction than conventional simple geometrical models. The results of this work can be utilized in wireless network planning. In the future, the same analysis should be done for different millimeter-wave frequency ranges.

References

AL-NUAIMI, M. and DING, M. (1994). Prediction models and measurements of microwave signals scattered from buildings. *IEEE Trans. Antennas Propagat.*, 42(8), pp. 1126-1137.

ALA-LAURINAHO, J., DU, Z., SEMKIN, V., VIIKARI, V., and RÄISÄNEN, A. V. (2015). Reflection coefficient method for antenna radiation pattern measurements. In: *European Radar Conference (EuRAD)*. Paris, pp. 285-288.

APPEL-HANSEN, J. (1973). Reflectivity level of radio anechoic chambers. *IEEE Trans. Antennas Propagat.*, 21(4), pp. 490-498.

BAHL, I. and BHARTIA, P. (1980). *Microstrip Antennas*. Dedham, Massachusetts: Artech House.

BALANIS, C. A. (2005). *Antenna Theory: Analysis and Design*. 3rd ed. Hoboken, N.J.: Wiley.

BEER, S. and ZWICK, T. (2010). Probe based radiation pattern measurements for highly integrated millimeter-wave antennas. In: *The 4th European Conference on Antennas and Propagation (EuCAP2010)*. Barcelona.

BEHDAD, N. and SARABANDI, K. (2006). A varactor-tuned dual-band slot antenna. *IEEE Trans. Antennas Propagat.*, 54(2), pp. 401-408.

BOGALE, T. and LE, L. (2016). Massive MIMO and mm-wave for 5G wireless HetNet: potential benefits and challenges. *IEEE Veh. Technol. Mag.*, 11(1), pp. 64-75.

BORN, M. and WOLF, E. (1970). *Principles of Optics*. 4th ed. Pergamon Press: Oxford.

BROWN, E. (1998). RF-MEMS switches for reconfigurable integrated circuits. *IEEE Trans. Microwave Theory Tech.*, 46(11), pp. 1868-1880.

CHENG, Y., XU, H., MA, D., WU, J., WANG, L., and FAN, Y. (2013). Millimeter-wave shaped-beam substrate integrated conformal array antenna. *IEEE Trans. Antennas Propagat.*, 61(9), pp. 4558-4566.

CHIAO, J., FU, Y., CHIO, I., DELISIO, M., and LIN, L. (1999). MEMS reconfigurable Vee antenna. In: *IEEE International Microwave Symposium Digest (MTT)*. Baltimore. pp. 1515-1518.

CHIREIX, H. (1936) "*Antennes à rayonnement zénithal réduit,*" L'Onde Electrique, 15, pp. 440–456.

CISCO (2016). Cisco visual networking index: global mobile data traffic forecast update, 2015-2020. *White paper*. Cisco, pp. 1-39.

CIVI, O., DEMIR, S., and AKIN, T. (2011). Reconfigurable antennas using RF-MEMS research in Turkey. In: *International Microwave Symposium Digest (MTT)*. Baltimore.

CURE, D., WELLER, T., PRICE, T., MIRANDA, F., and VAN KEULS, F. (2014). Low-profile tunable dipole antenna using barium strontium titanate varactors. *IEEE Trans. Antennas Propagat.*, 62(3), pp. 1185-1193.

DE LUIS, J. and DE FLAVIIS, F. (2009). A reconfigurable dual frequency switched beam antenna array and phase shifter using PIN diodes. In: *IEEE Antennas and Propagation Society International Symposium*. Charleston.

DEGLI-ESPOSTI, V. and BERTONI, H. (1999). Evaluation of the role of diffuse scattering in urban microcellular propagation. In: *IEEE VTS 50th Vehicular Technology Conference (VTC1999)*. Amsterdam, pp. 1392-1396.

DEGLI-ESPOSTI, V., FUSCHINI, F., VITUCCI, E., and FALCIASECCA, G. (2007). Measurement and modelling of scattering from buildings. *IEEE Trans. Antennas Propagat.*, 55(1), pp. 143-153.

DEGLI-ESPOSTI, V., FUSCHINI, F., VITUCCI, E., BARBIROLI, M., ZOLI, M., TIAN, L., YIN, X., DUPLEICH, D., MULLER, R., SCHNEIDER, C., and THOMA, R. (2014). Ray-tracing-based mm-wave beamforming assessment. *IEEE Access*, 2, pp. 1314-1325.

DESCHAMPS, G. (1953). Microstrip microwave antennas. In: *The 3rd USAF symposium on Antennas*.

DI PALMA, L., CLEMENTE, A., DUSSOPT, L., SAULEAU, R., POTIER, P., and POLIGUEN, P. (2015). 1-Bit unit-cell for transmitarray applications in Ka-band. In: *9th European Conference on Antennas and Propagation (EuCAP2015)*. Lisbon.

DICKEY, M., LAZZI, G., SO, J., THELEN, J., QUSBA, A., and HAYES, G. (2013). *Reversibly Deformable and Mechanically Tunable Fluidic Antennas*. Patent US 8587493 B2.

DIDASCALOU, D., DOTTLING, M., GENG, N., and WIESBECK, W. (2003). An approach to include stochastic rough surface scattering into deterministic ray-optical wave propagation modeling. *IEEE Trans. Antennas Propagat.*, 51(7), pp. 1508-1515.

DOTTLING, M., KUCHEN, F., and WIESBECK, W. (1997a). Deterministic modeling of the street canyon effect in urban micro and pico cells. In: *IEEE International Conference on Communications*. Montreal: IEEE, pp. 36-40.

DOTTLING, M., ZWICK, T., and WIESBECK, W. (1997b). Ray tracing and imaging techniques in urban pico and micro cell wave propagation modelling. In: *10th IET International Conference on Antennas and Propagation*. Edinburgh, pp. 311-315.

EMERSON, D. (1998). Jagadis Chandra Bose: millimetre wave research in the nineteenth century. In: *Region 10th International Conference on Global Connectivity in Energy, Computer, Communication and Control*. New Delhi, pp. 282-287.

ERDIL, E., TOPALLI, K., UNLU, M., CIVI, O., and AKIN, T. (2007). Frequency tunable microstrip patch antenna using RF MEMS technology. *IEEE Trans. Antennas Propagat.*, 55(4), pp. 1193-1196.

ERDIL, E., TOPALLI, K., ZORLU, Ö., TORAL, T., YILDIRIM, E., KULAH, H., and CIVI, O. (2013). A reconfigurable microfluidic transmitarray unit cell. In: *The 7th European Conference on Antennas and Propagation (EuCAP2013)*. Gothenburg, pp. 2957-2960.

ETSI TS 102 524 (2006). *Fixed radio systems; point-to-point equipment; radio equipment and antennas for use in point-to-point millimetre wave applications in the fixed services (mmwFS) frequency bands 71 GHz to 76 GHz and 81 GHz to 86 GHz.* July. Sophia Antipolis: European Telecommunications Standards Institute, pp. 1-19.

FAYAD, H. and RECORD, P. (2006). Broadband liquid antenna. *Electron. Lett.*, 42(3), pp. 133-134.

FCC (1997). *Millimeter Wave Propagation: Spectrum Management Implications*. FCC memorandum opinion and order. Washington, DC: Federal Communications Comission, pp. 1-39.

FCC (2005). *Allocations and service rules for the 71-76 GHz, 81-86 GHz, and 92-95 GHz bands*. Bulletin Number 70, July. Washington, DC: Federal Communications Comission, pp. 1-24

FRIIS, H. (1946). A note on a simple transmission formula. *Proceedings of the IRE*, 34(5), pp. 254-256.

FRIIS, H. and FELDMAN, C. (1937). A multiple unit steerable antenna for short-wave reception. *Bell System Technical Journal*, 16(3), pp. 337-419.

FRIIS, H., FELDMAN, C., and SHARPLESS, W. (1934). The determination of the direction of arrival of short radio waves. *Proceedings of the IRE*, 22(1), pp. 47-78.

FUGEN, T., KNORZER, S., LANDMANN, M., THOMA, R., and WIESBECK, W. (2007). A 3-D ray tracing model for macrocell urban environments and its verification with measurements. In: *The 2nd European Conference on Antennas and Propagation (EuCAP2007)*. Edinburgh.

FUSCHINI, F., EL-SALLABI, H., DEGLI-ESPOSTI, V., VUOKKO, L., GUIDUCCI, D., and VAINIKAINEN, P. (2008). Analysis of multipath propagation in urban environment through multidimensional measurements and advanced ray tracing simulation. *IEEE Trans. Antennas Propagat.*, 56(3), pp. 848-857.

GHADDAR, M., TALBI, L., DENIDNI, T., and SEBAK, A. (2007). A conducting cylinder for modeling human body presence in indoor propagation channel. *IEEE Trans. Antennas Propagat.*, 55(11), pp. 3099-3103.

GSCHWENDTNER, B., WÖLFLE, G., BURK, B., and LANDSTORFER, F. (1995). Ray tracing vs. ray launching in 3-d microcell modelling. In: *The 1st European Personal and Mobile Communications Conference (EPMCC)*. pp. 74-79.

GUSTAFSON, C. and TUFVESSON, F. (2012). Characterization of 60 GHz shadowing by human bodies and simple phantoms. *Radioengineering*, 21(4), pp. 979-984.

GUTTON, H. and BAISSINOT, G. (1955). *Flat Aerial for Ultra High Frequencies*. French patent no. 703 113.

HALL, M., BARCLAY, L., and HEWITT, M. (1996). *Propagation of Radiowaves*. London: Institution of Electrical Engineers.

HAMMERSTAD, E. (1975). Equations for microstrip circuit design. In: *The 5th European Microwave Conference*. Hamburg, pp. 268-272.

HAUPT, R. and LANAGAN, M. (2013). Reconfigurable antennas. *IEEE Antennas and Propagation Magazine*, 55(1), pp. 49-61.

HERTZ, H. (1887). Ueber sehr schnelle electrische Schwingungen. *Ann. Phys. Chem.*, 267(7), pp. 421-448.

HOWELL, J. (1975). Microstrip antennas. *IEEE Trans. Antennas Propagat.*, 23(1), pp. 90-93.

HUANG, K. and WANG, Z. (2011). *Millimeter Wave Communication Systems*. Hoboken, N.J.: Wiley.

HUAWEI (2013). *5G: a technology vision*. Huawei Technologies, pp. 1-16.

HUM, S. and PERRUISSEAU-CARRIER, J. (2014). Reconfigurable reflectarrays and array lenses for dynamic antenna beam control: a review. *IEEE Trans. Antennas Propagat.*, 62(1), pp. 183-198.

HUR, S., BAEK, S., KIM, B., CHANG, Y., MOLISCH, A., RAPPAPORT, T., HANEDA, K., and PARK, J. (2016). Proposal on millimeter-wave channel modeling for 5G cellular system. *IEEE Journal of Selected Topics in Signal Process*, doi 10.1109/JSTSP.2016.2527364.

HYYPPÄ, J. (2011). State of the art in laser scanning. In: *Photogrammetric Week 2011*. Wichmann/VDE Verlag. Berlin & Offenbach, pp. 203-216.

IEEE (1993). *Standard Definition of Terms for Antennas*. New York: Institute of Electrical and Electronics Engineers, 1993.

IEEE802.15.3C (2009). *Part 15.3: Wireless Medium Access Control (MAC) and Physical Layer (PHY) Specifications for High Rate Wireless Personal Area Networks (WPANs), Amendment 2: Millimeter-wave-based Alternative Physical Layer Extension*. Oct. New York: Institute of Electrical and Electronics Engineers, pp. 1-187.

IEEE802.11.AD (2012). *Part 11: Wireless LAN Medium Access Control (MAC) and Physical Layer (PHY) Specifications, Amendment 3: Enhancements for very high throughput in the 60 GHz band*. Dec. New York: Institute of Electrical and Electronics Engineers, pp. 1-597.

ISKANDER, M., YUN, Z., and ZHANG, Z. (2001). Outdoor/indoor propagation modeling for wireless communications systems. In: *IEEE Antennas and Propagation Society International Symposium*. Boston, pp. 150-153.

JACOB, M., PRIEBE, S., KÜRNER, T., PETER, M., WISOTZKI, M., FELBECKER, R., and KEUSGEN, W. (2013). Extension and validation of the IEEE 802.11ad 60 GHz human blockage model. In: The *7th European Conference on Antennas and Propagation (EuCAP2013)*. Gothenburg, pp. 2806-2810.

JACOB, M., PRIEBE, S., MALTSEV, A., LOMAYEV, A., ERCEG, V., and KÜRNER, T. (2011). A ray tracing based stochastic human blockage model for the IEEE 802.11ad 60 GHz channel model. In: *The 5th European Conference on Antennas and Propagation (EuCAP2011)*. Rome, pp. 3084-3088.

JOSEFSSON, L. and PERSSON, P. (2006). *Conformal Array Antenna Theory and Design*. New Jersey: IEEE Press, Wiley.

KELLER, J. (1962). Geometrical theory of diffraction. *Journal of the Optical Society of America*, 52(2), pp. 116-130.

KHAIRKAR, G., ALA-LAURINAHO, J., VIIKARI, V., SEMKIN, V., and RÄISÄNEN, A. V. (2016). Mitigation of multiple reflections in antenna pattern retrieval method. In: *The 10th European Conference on Antennas and Propagation*. Davos.

KIM, B., PAN, B., NIKOLAOU, S., KIM, Y., PAPAPOLYMEROU, J., and TENTZERIS, M. (2008). A novel single-feed circular microstrip antenna with reconfigurable polarization capability. *IEEE Trans. Antennas Propagat.*, 56(3), pp. 630-638.

KINGSLEY, N., ANAGNOSTOU, D., TENTZERIS, M., and PAPAPOLYMEROU, J. (2007). RF MEMS sequentially reconfigurable Sierpinski antenna on a flexible organic substrate with novel DC-biasing technique. *Journal of Microelectromechanical Systems*, 16(5), pp. 1185-1192.

KIPP, R. A. and MILLER, M. C. (2004). Shooting-and-bouncing ray method for 3D indoor wireless propagation in WLAN applications. In: *IEEE Antennas and Propagation Society International Symposium*. California, pp. 1639-1642.

KLINE, M. (1951). An asymptotic solution of Maxwell's equations. *Communications on Pure and Applied Mathematics*, 4(2-3), pp. 225-262.

KLOCH, C. and BACH ANDERSEN, J. (1997). Radiosity-an approach to determine the effect of rough surface scattering in mobile scenarios. In: *Digest of IEEE Antennas and Propagation Society International Symposium*. Montreal, pp. 890-893.

KNUDSEN, H. (1953). The field radiated by a ring quasi-array of an infinite number of tangential or radial dipoles. *Proceedings of the IRE*, 41(6), pp. 781-789.

KOUYOUMJIAN, R. and PATHAK, P. (1974). A uniform geometrical theory of diffraction for an edge in a perfectly conducting surface. *Proceedings of the IEEE*, 62(11), pp. 1448-1461.

KRAUS, K. (2007). *Photogrammetry*. Berlin: Walter De Gruyter.

KUNISCH, J. and PAMP, J. (2008). Ultra-wideband double vertical knife-edge model for obstruction of a ray by a person. In: *IEEE International Conference on Ultra-Wideband*. Hannover, pp. 17-20.

KYRÖ, M., KOLMONEN, V., and VAINIKAINEN, P. (2012). Experimental propagation channel characterization of mm-wave radio links in urban scenarios. *IEEE Antennas and Wireless Propag. Lett.*, 11, pp. 865-868.

LAMBA, A., YADAV, J., and DEVI, G. (2012). Analysis of technologies in 3G and 3.5G mobile networks. In: *International Conference on Communication Systems and Network Technologies (CSNT2012)*. Rajkot, pp. 330-333.

LANGEN, B., LOBER, G., and HERZIG, W. (1994). Reflection and transmission behaviour of building materials at 60 GHz. In: *IEEE 5th Int. Symp. Personal, Indoor and Mobile Radio Communications (PIMRC1994)*, 2, pp. 505–509.

LEBERL, F., IRSCHARA, A., POCK, T., MEIXNER, P., GRUBER, M., SCHOLZ, S., and WIECHERT, A. (2010). Point clouds: lidar versus 3D vision. *Photogrammetric Engineering and Remote Sensing*, 76(10), pp. 1123-1134.

LIANG, G. and BERTONI, H. (1997). A new approach to 3D ray tracing for site specific propagation modeling. In: *47th IEEE Vehicular Technology Conference*. Phoenix, pp. 1113-1117.

LIBERTY, J., RAPPAPORT, T. (1996). A geometrically based model for line-of-sight multipath radio channels. In: *Proc. 46th IEEE Veh. Technol. Conf*. Atlanta. pp. 844-848.

LIU, M., FENG, Z., and WU, Q. (2008). A millimeter-wave cylindrical conformal phased microstrip antenna array. In: *China-Japan Joint Microwave Conference*. Shanghai, pp. 150-153.

LIU, Z. and WANG, C. (2012). Shooting and bouncing ray and physical optics for predicting the EM scattering of coated PEC objects. In: *IEEE Asia-Pacific Conference on Antennas and Propagation (APCAP2012)*. Singapore, pp. 104-105.

LUNEBERG, R. (1944). *Mathematical Theory of Optics*. Brown University Press.

MAILLOUX, R. (2005). *Phased Array Antenna Handbook*. Boston: Artech House.

MATTHEWS, E., CUCCIA, C., and RUBIN, M. (1979). Technology considerations for the use of multiple beam antenna systems in communication satellites. *IEEE Trans. on Microwave Theory Tech.*, 27(12), pp. 998-1004.

MAXWELL, J. C. (1865). A dynamical theory of the electromagnetic field. *Philosophical Transactions of the Royal Society of London*, 155, pp. 459-512.

MCKOWN, J. and HAMILTON, R. (1991). Ray tracing as a design tool for radio networks. *IEEE Network*, 5(6), pp. 27-30.

MITTRA, R. (2014). *Computational Electromagnetics*. New York: Springer.

MOHTASHAMI, V. and SHISHEGAR, A. (2010). Accuracy and computational efficiency improvement of ray tracing using line search theory. *IET Microw. Antennas Propag.*, 4(9), pp. 1290-1299.

MOLISCH, A. (2011). *Wireless Communications*. Chichester, West Sussex, U.K.: Wiley.

MUNSON, R. (1972). Microstrip phased array antennas. In: *Proc. of Twenty-Second Symp. on USAF Antenna Research and Development Program*.

MUNSON, R. (1974). Conformal microstrip antennas and microstrip phased arrays. *IEEE Trans. Antennas Propagat.*, 22(1), pp. 74-78.

NOAA, National Oceanic and Atmospheric Administration Coastal Services Center (2012). *Lidar 101: an introduction to Lidar technology, data, and applications*. Revised. Charleston, SC: NOAA Coastal Services Center, pp. 1-76.

NIKOLAOU, S., BAIRAVASUBRAMANIAN, R., LUGO, C., CARRASQUILLO, I., THOMPSON, D., PONCHAK, G., PAPAPOLYMEROU, J., and TENTZERIS, M. (2006). Pattern and frequency reconfigurable annular slot antenna using PIN diodes. *IEEE Trans. Antennas Propagat.*, 54(2), pp. 439-448.

NUCKELT, J., ROSE, D., JANSEN, T., and KÜRNER, T. (2013). On the use of OpenStreetMap data for V2X channel modeling in urban scenarios. In: The *7th European Conference on Antennas and Propagation (EuCAP2013)*. Göteborg, pp. 3984-3988.

PIX4D (2014). White paper – how accurate are UAV surveying methods?. *White paper*. Pix4D, pp. 1-8.

POP, G. and BUCKSCH, A. (2007). Combining modern techniques for urban 3D modelling. In: *IEEE International Geoscience and Remote Sensing Symposium*. Barcelona, pp. 2067-2070.

POZAR, D. (1992). Microstrip antennas. *Proceedings of the IEEE*, 80(1), pp. 79-91.

PRIEBE, S., JACOB, M., and KÜRNER, T. (2012). Calibrated broadband ray tracing for the simulation of wave propagation in mm and sub-mm wave indoor communication channels. In: *The 18th European Wireless Conference*. Poznan.

PRINGLE, L., HARMS, P., BLALOCK, S., KIESEL, G., KUSTER, E., FRIEDERICH, P., PRADO, R., MORRIS, J., and SMITH, G. (2004). A reconfigurable aperture antenna based on switched links between electrically small metallic patches. *IEEE Trans. Antennas Propagat.*, 52(6), pp. 1434-1445.

RÄISÄNEN, A. V., ALA-LAURINAHO, J., HANEDA, K., JÄRVELÄINEN, J., KARTTUNEN, A., SEMKIN, V., LAMMINEN, A., and SÄILY, J. (2013). Studies on E-band antennas and propagation. In: *Loughborough Antennas and Propagation Conference (LAPC2013)*. Loughborough, pp. 176-180.

RANVIER, S., KYRÖ, M., ICHELN, C., LUXEY, C., STARAJ, R., and VAINIKAINEN, P. (2009). Compact 3-D on-wafer radiation pattern measurement system for 60 GHz antennas. *Microwave and Optical Technology Letters*, 51(2), pp. 319-324.

RAUTIAINEN, T., HOPPE, R. and WOLFLE, G. (2007). Measurements and 3D ray tracing propagation predictions of channel characteristics in indoor environments. In: *The 18th IEEE International Symposium on Personal, Indoor and Mobile Radio Communications*. Athens.

REBEIZ, G. (2003). *RF MEMS*. Hoboken, NJ: J. Wiley.

ROSE, D. and KÜRNER, T. (2014). An analytical 3D ray-launching method using arbitrary polygonal shapes for wireless propagation prediction. In: *The 80th IEEE Vehicular Technology Conference (VTC2014-Fall)*. Vancouver.

SÁEZ DE ADANA, F. (2011). *Practical Applications of Asymptotic Techniques in Electromagnetics*. Boston, Mass.: Artech House.

SATO, R., SATO, H., and SHIRAI, H. (2005). A SBR estimation for indoor wave propagation through dielectric walls. In: *IEEE Antennas and Propagation Society International Symposium*. pp. 719-722.

SEMKIN, V., KYRÖ, M., KOLMONEN, V., LUXEY, C., BISOGNIN, A., FERRERO, F., HAPPY, H., and RÄISÄNEN, A. V. (2013a). Conformal antenna array for 60 GHz applications. In: *The 7th European Conference on Antennas and Propagation (EuCAP2013)*. Göteborg, pp. 605-608.

SEMKIN, V., KYRÖ, M., KOLMONEN, V., LUXEY, C., BISOGNIN, A., FERRERO, F., HAPPY, H., and RÄISÄNEN, A. V. (2013b). Antenna array for mm-wave communications bent on the cylindrical shape object. In: *XXXIII Finnish URSI Convention on Radio Science and SMARAD Seminar*. Espoo, pp. 39-42.

SIMMONS, A., GIDDINGS, O., DIAMOND, M., and GINDSBERG, J. (1966). A multiple-beam two-dimensional waveguide slot array. In: *International Convention Record (IRE1958)*. New York, pp. 56-69.

SINGH, S., ZILIOTTO, F., MADHOW, U., BELDING, E., and RODWELL, M. (2009). Blockage and directivity in 60 GHz wireless personal area networks: from cross-layer model to multihop MAC design. *IEEE J. Select. Areas Commun.*, 27(8), pp. 1400-1413.

SO, J., THELEN, J., QUSBA, A., HAYES, G., LAZZI, G., and DICKEY, M. (2009). Reversibly deformable and mechanically tunable fluidic antennas. *Adv. Funct. Mater.*, 19(22), pp. 3632-3637.

SOMMERFELD, A. and RUNGE, J. (1911). Anwendung der Vektorrechnung auf die Grundlagen der geometrischen Optik. *Ann. Phys.*, 340(7), pp. 277-298.

TAWK, Y., ALBRECHT, A., HEMMADY, S., BALAKRISHNAN, G., and CHRISTODOULOU, C. (2010). Optically pumped frequency reconfigurable antenna design. *Antennas Wirel. Propag. Lett.*, 9, pp. 280-283.

TITZ, D., FERRERO, F., and LUXEY, C. (2012). Development of a millimeter-wave measurement setup and dedicated techniques to characterize the matching and radiation performance of probe-fed antennas. *IEEE Antennas and Propagation Magazine*, 54(4), pp. 188-203.

VASYLCHENKO, A., FARSEROTU, J., FERNÁNDEZ-BOLAÑOS, M., IONESCU, A., BREBELS, S., DE RAEDT, W., and VANDENBOSCH, G. (2011). Scalable conformal array for multi-gigabit body centric wireless communication. In: *The 5th IEEE International Symposium on Medical Information and Communication Technology*. Montreux, pp. 74-78.

VAUGHAN, R. and BACH ANDERSEN, J. (2003). *Channels, Propagation and Antennas for Mobile Communications*. London: Institution of Electrical Engineers.

VIIKARI, V., DU, Z., SEMKIN, V., ALA-LAURINAHO, J., and RÄISÄNEN, A. V. (2015). Reflection coefficient method for characterizing antennas on probe stations. In: The *9th European Conference on Antennas and Propagation (EuCAP)*. Lisbon.

WHITE, C. and REBEIZ, G. (2009). Single- and dual-polarized tunable slot-ring antennas. *IEEE Trans. Antennas Propagat.*, 57(1), pp. 19-26.

ZWICK, T., BACKS, C., PFEIFFER, U., LIU, D., and GAUCHER, B. (2004). Probe based MMW antenna measurement setup. In: *IEEE Antennas and Propagation Society International Symposium*. pp. 747-750.

In a modern society a lot of digital content is being uploaded and downloaded from different digital services using wireless access. The increasing interest in high date rate communications brings new challenges for researchers. Reconfigurable antennas, with the ability to control their properties according to the changes in the environment, can help to improve the overall system performance and increase the system capacity. Furthermore, studies of radio wave propagation and channel modeling can help in careful planning and deployment of the wireless communication systems. In this thesis both of these relevant research topics are addressed.

BUSINESS +
ECONOMY

ART +
DESIGN +
ARCHITECTURE

SCIENCE +
TECHNOLOGY

CROSSOVER

DOCTORAL
DISSERTATIONS